

# UC Irvine

## UC Irvine Previously Published Works

### Title

Ovol1/2 loss-induced epidermal defects elicit skin immune activation and alter global metabolism

### Permalink

<https://escholarship.org/uc/item/8ws5q1wj>

### Journal

EMBO Reports, 24(7)

### ISSN

1469-221X

### Authors

Dragan, Morgan

Chen, Zeyu

Li, Yumei

et al.

### Publication Date








2023-07-05

### DOI

10.15252/embr.202256214

Peer reviewed

# *Ovol1/2* loss-induced epidermal defects elicit skin immune activation and alter global metabolism

Morgan Dragan<sup>1,2</sup> , Zeyu Chen<sup>1,†,‡</sup>, Yumei Li<sup>1</sup> , Johnny Le<sup>1</sup> , Peng Sun<sup>1</sup>, Daniel Haensel<sup>1,§</sup> , Suhas Sureshchandra<sup>3</sup>, Anh Pham<sup>1</sup> , Eddie Lu<sup>1</sup>, Katherine Thanh Pham<sup>1</sup>, Amandine Verlande<sup>1</sup> , Remy Vu<sup>1,2</sup>, Guadalupe Gutierrez<sup>1</sup>, Wei Li<sup>1</sup>, Cholsoon Jang<sup>1</sup>, Selma Masri<sup>1</sup> & Xing Dai<sup>1,2,4,\*</sup> 

## Abstract

Skin epidermis constitutes the outer permeability barrier that protects the body from dehydration, heat loss, and myriad external assaults. Mechanisms that maintain barrier integrity in constantly challenged adult skin and how epidermal dysregulation shapes the local immune microenvironment and whole-body metabolism remain poorly understood. Here, we demonstrate that inducible and simultaneous ablation of transcription factor-encoding *Ovol1* and *Ovol2* in adult epidermis results in barrier dysregulation through impacting epithelial-mesenchymal plasticity and inflammatory gene expression. We find that aberrant skin immune activation then ensues, featuring Langerhans cell mobilization and T cell responses, and leading to elevated levels of secreted inflammatory factors in circulation. Finally, we identify failure to gain body weight and accumulate body fat as long-term consequences of epidermal-specific *Ovol1/2* loss and show that these global metabolic changes along with the skin barrier/immune defects are partially rescued by immunosuppressant dexamethasone. Collectively, our study reveals key regulators of adult barrier maintenance and suggests a causal connection between epidermal dysregulation and whole-body metabolism that is in part mediated through aberrant immune activation.

**Keywords** epidermis; epithelial-mesenchymal plasticity (EMP); immune; metabolism; *Ovol1/Ovol2*

**Subject Categories** Immunology; Metabolism; Signal Transduction

**DOI** 10.15252/embr.202256214 | Received 2 October 2022 | Revised 29 April 2023 | Accepted 10 May 2023 | Published online 30 May 2023

**EMBO Reports (2023) 24: e56214**

## Introduction

Skin is a vital outer barrier that protects the body from water/heat loss and myriad environmental assaults. It is also the largest organ in the

body, constituting ~10–15% of body weight and regulates important aspects of physiology such as body temperature. Within skin, terminal differentiation of epidermal cells produces stratum corneum—a lipid-rich physical permeability barrier, while immune cells such as tissue-resident Langerhans cells (LCs), gamma delta T ( $\gamma\delta$ T) lymphocytes, and macrophages collectively provide an immunological barrier to fend off pathogens, resolve insults, and/or repair damage (Elias, 2007; Chambers & Vukmanovic-Stejić, 2020; Niec *et al.*, 2021). Barrier defects are associated with inflammatory skin diseases such as psoriasis and atopic dermatitis (Proksch *et al.*, 2006; Elias & Wakefield, 2014; Dainichi *et al.*, 2018). Moreover, tantalizing links exist between skin inflammation and whole-body perturbation, evident through higher incidence of psoriasis and atopic dermatitis in patients with obesity (Zheng, 2014; Brunner *et al.*, 2017), growth failure in patients with ichthyosis the clinical severity of which parallels the extent of barrier dysfunction (Dereksson *et al.*, 2012; Elias *et al.*, 2012; Yamamoto *et al.*, 2020), and weight loss in animals following acute inflammation (Gabay & Kushner, 1999; de Oliveira *et al.*, 2022). However, little is known about how epidermal/barrier dysregulation shapes the skin immune microenvironment in the absence of any blatant disease-inducing stimuli, and how skin defects instigate whole-body physiological and metabolic changes.

Genetic mechanisms that regulate embryonic epidermal development and barrier acquisition have been well-studied (Hardman *et al.*, 1998; Segre, 2006). Transcriptional repressor-encoding homologs *Ovol1* and *Ovol2* are among the more recently identified regulators of barrier development, and they function in part through modulating the epithelial-mesenchymal plasticity of embryonic epidermal cells (MacKay *et al.*, 2006; Nair *et al.*, 2006; Teng *et al.*, 2007; Wells *et al.*, 2009; Watanabe *et al.*, 2014; Lee *et al.*, 2014a; Sha *et al.*, 2019; Vu *et al.*, 2022a). *Ovol1* is normally expressed in differentiating epidermal keratinocytes, and germline loss of *Ovol1* causes embryonic epidermal hyperproliferation and a transient delay in barrier acquisition (Nair *et al.*, 2006; Teng *et al.*, 2007). In adult stage, *Ovol1*-deficient mice are more susceptible to imiquimod-induced psoriasis-like inflammation,

<sup>1</sup> Department of Biological Chemistry, School of Medicine, University of California, Irvine, CA, USA

<sup>2</sup> The NSF-Simons Center for Multiscale Cell Fate Research, University of California, Irvine, CA, USA

<sup>3</sup> Department of Physiology and Biophysics, School of Medicine, University of California, Irvine, CA, USA

<sup>4</sup> Department of Dermatology, School of Medicine, University of California, Irvine, CA, USA

\*Corresponding author. Tel: +949 824 3101; Fax: +949 824 2688; E-mail: xdai@uci.edu

<sup>†</sup>Present address: Department of Dermatology, Shanghai Tenth People's Hospital, Tongji University School of Medicine, Shanghai, China

<sup>‡</sup>Present address: Institute of Psoriasis, Tongji University School of Medicine, Shanghai, China

<sup>§</sup>Present address: Program in Epithelial Biology, Stanford University School of Medicine, Stanford, CA, USA

but otherwise do not show remarkable perturbation in skin homeostasis (Sun *et al.*, 2021; Dragan *et al.*, 2022). *Ovol2* is normally expressed in epidermal basal stem/progenitor cells, and *Ovol2*-deficient mice show delayed wound closure with compromised directional migration while their epidermal development and homeostasis remain largely intact (Haensel *et al.*, 2019). Despite these seemingly different expression patterns and functions, *Ovol1* and *Ovol2* are also known to play redundant/compensatory roles and the loss of one stimulates the expression of another (Teng *et al.*, 2007; Lee *et al.*, 2014a). *K14-Cre*-directed, simultaneous ablation of *Ovol1* and *Ovol2* in embryonic epidermis disrupts barrier formation and keratinocyte adhesion/differentiation due to elevated expression of genes associated with epithelial-mesenchymal transition (EMT), an extreme form of epithelial-mesenchymal plasticity, leading to perinatal lethality (Lee *et al.*, 2014a).

Compared with developing embryonic skin, postnatal skin is more heavily exposed to myriad environmental aggressors (Proksch *et al.*, 2006; Segre, 2006; Natsuga, 2014). Not only the structure, composition, and immune microenvironment of the skin but also barrier strength, turnover rate, differentiation trajectory, and molecular makeup of the epidermis differ considerably between embryonic and adult skin (Moulin *et al.*, 2001; Oranges *et al.*, 2015; Rognoni *et al.*, 2018; Haensel *et al.*, 2020; Lin *et al.*, 2020; Henneke *et al.*, 2021; Moretti *et al.*, 2022). Thus, it is necessary to experimentally test whether the molecular mechanisms, for example, *Ovol1/2* suppression of the EMT gene expression program, that govern epidermal development are also required for adult barrier maintenance. Mice that cannot maintain a robust barrier during homeostasis also offer useful models to assess the local immunological and whole-body metabolic consequences of epidermal dysregulation in environmentally exposed skin.

Here, we employed an inducible approach to delete both *Ovol1* and *Ovol2* specifically in adult epidermis. Our results uncovered a critical role for *Ovol1/2* in epidermal barrier maintenance and terminal differentiation. Through gene expression and chromatin immunoprecipitation (ChIP)-seq analyses, we found that *Ovol1* and *Ovol2* not only regulate common downstream target genes involved in EMT/cell adhesion control but also directly regulate inflammatory genes. We identified precocious epidermal LC mobilization and aberrant T cell responses as local, and failure to gain body weight and accumulate body fat as whole-body, consequences of epidermal *Ovol1/2* deletion. Finally, we showed that immunosuppressive agent dexamethasone (Dex) can partially normalize aberrant skin immune activation and restore weight/fat gain in *Ovol1/2*-deficient mice. Together, our findings not only reveal key regulators of adult epidermal barrier maintenance but also suggest a causal link between epidermal dysregulation and whole-body metabolism that is in part mediated through aberrant immune activation.

## Results

### Inducible and epidermal-specific deletion of *Ovol1* and *Ovol2* in adult skin results in defective barrier, disrupted cell–cell adhesion, and aberrant terminal differentiation

To ask whether adult skin requires *Ovol* genes for barrier maintenance during homeostasis, we generated tamoxifen (TAM)-

inducible double knockout or iDKO (*K14-CreER;Ovol1<sup>f/f</sup>;Ovol2<sup>f/f</sup>*) mice to enable the simultaneous deletion of *Ovol1* and *Ovol2* in adult epidermis. Successful deletion of both genes was evident through reduced expression of *Ovol1* and *Ovol2* mRNAs after TAM injection (Fig EV1A and B).

Prior to TAM induction, adult iDKO mice showed no detectable difference from their control littermates in back skin trans-epidermal water loss (TEWL), suggesting normal barrier function before gene deletion (Fig 1A). Following TAM injections, both iDKO mice and their littermates with various control genotypes exhibited a trend of increased TEWL especially starting at ~ 15 days post-first injection (DPI), soon after one full epidermal turnover cycle (Koster, 2009; Fig 1A). However, TEWL values were consistently and significantly higher in iDKO mice than in control littermates throughout the course of measurement (90 DPI; Fig 1A).

To understand the nature of the barrier defect, we performed morphological and lipidomics analyses to examine the structural and biochemical integrity of the iDKO epidermis. Both histology and transmission electron microscopy (TEM) revealed disrupted cell–cell adhesion between, and abnormal nuclear morphology of, epidermal basal/suprabasal cells in iDKO mice but not control littermates by 15 DPI (Fig 1B–D). Immunostaining of epidermal sheets from control and iDKO mice for adherence junction component  $\beta$ -catenin revealed reduced membrane signals in iDKO samples (Fig 1E and F). Additionally, iDKO epidermal granular cells showed altered morphology of keratohyalin granules (Fig 1D), suggesting abnormal terminal differentiation (Hooper & Eggink, 2022). Lipidomics on trypsin-isolated epidermis revealed a significantly decreased production of triacylglycerol (50:3) and urocanic acid, which are known to occur with skin barrier defect (Choi & Maibach, 2005; Fluhr *et al.*, 2010), in iDKO epidermis at 52 DPI compared with control littermates (Fig 1G and H). Decreases in other metabolites associated with cellular stress and skin barrier, such as hypoxanthine and ceramide-dihydro (d18:0/26:0; Coderch *et al.*, 2003; Kim *et al.*, 2017), were not statistically significant (Fig EV1C and D; Dataset EV1). Collectively, these findings demonstrate that *Ovol1* and *Ovol2* are required in adult skin for robust epidermal barrier maintenance, proper cell–cell adhesion, and optimal terminal differentiation.

Compared with back skin, mouse paw skin faces more physical abrasion and mechanical stress. Starting at ~ 30 DPI, the iDKO mice showed visibly elongated toenails which became exacerbated over time, and underneath the nails, we frequently observed blood clots (Figs 1I and EV1E). iDKO paw pads appeared more calloused and contained darker pigmentation, and their paws and toes significantly enlarged compared with the control counterparts (Figs 1I and J, and EV1E and F). Sagittal sections through the toes revealed expanded toe pad epithelia and elongated nail plate, but no difference in nail matrix (Figs 1K and EV1G–J). While immunofluorescence using antibodies against Ki67, K14, K1, loricrin, or filaggrin failed to reveal remarkable alterations in toe pad epidermal cell proliferation and early differentiation, the filaggrin-positive compartment in iDKO toe pads was expanded and the average size of their filaggrin-positive granules was significantly increased compared with the control counterparts (Figs 1L and M, and EV1K–Q). As such, terminal differentiation of the paw epidermis is likely also perturbed by loss of *Ovol1* and *Ovol2*, reminiscent of the defect in back skin epidermis.

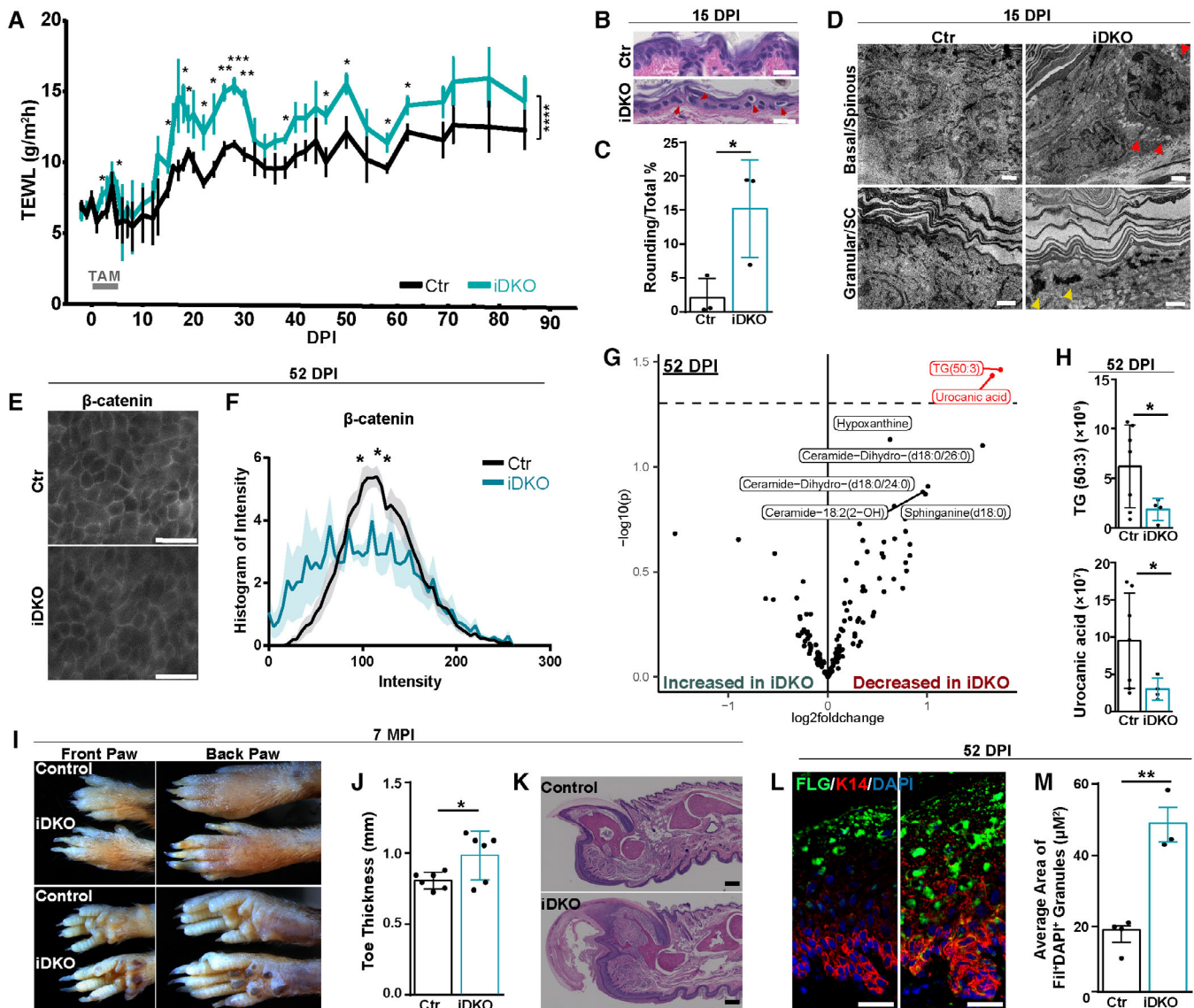


**Figure 1. Induced deletion of *Ovol1/2* in adulthood leads to skin epidermal and toe defects.**

- A Time course of TEWL measurements in control and iDKO mice prior to (–2 – 0 DPI) and following TAM injections.  $n = 4$  biological replicates per genotype.
- B Representative H/E images of epidermis from control and iDKO mice at 15 DPI.
- C Quantitative analysis of epidermal cell rounding from (B).  $n = 3$  biological replicates per genotype.
- D Representative TEM images of control and iDKO mice at 15 DPI. Red arrows point to gaps in cellular adhesion and yellow arrows point to abnormal keratohyalin granules. SC, stratum corneum.
- E, F Representative images (E) and quantification (F) of whole-mount immunostaining of  $\beta$ -catenin. Control:  $n = 7$  biological replicates; iDKO:  $n = 5$  biological replicates.
- G Volcano plot of differential lipid contents between control and iDKO epidermis.
- H Ion counts of the indicated lipid species. Control:  $n = 7$  biological replicates; iDKO:  $n = 4$  biological replicates.
- I Representative images of the paws of control and iDKO mice at 7 MPI.
- J Quantification of toe thickness in control and iDKO mice ( $n = 6$  biological replicates per genotype).
- K Representative H/E images of toes at 7 MPI.
- L Representative immunofluorescent images of the toe pad for filaggrin (Flg). K14 marks basal keratinocytes and DAPI marks nuclei.
- M Quantification of the average size of filaggrin<sup>+</sup> deposits at 52 DPI as shown in (L).  $n = 3$  biological replicates per genotype.

Data information: Scale bar: 20  $\mu\text{m}$  in (B) and (E), 1  $\mu\text{m}$  in (D), 250  $\mu\text{m}$  in (K), and 25  $\mu\text{m}$  in (L). For (A, F), data are represented as mean  $\pm$  SEM (error bars in A and shaded areas in F). Two-way ANOVA and Student's paired  $t$ -test with two tails were performed for (A), while Sidak's multiple comparisons test for individual points was performed for (F). For (C, E, F, H, J, M), data are represented as mean  $\pm$  SD and statistical analysis was done with the Holm–Sidak method. \* $P \leq 0.05$ ; \*\* $P \leq 0.005$ ; \*\*\* $P \leq 0.0005$ ; \*\*\*\* $P \leq 0.00005$ .

Source data are available online for this figure.

## Gene expression analyses corroborate known function of *Ovol1/2* in epithelial-mesenchymal plasticity and implicate their new roles in inflammatory gene expression

Terminal differentiation abnormality in iDKO mice may reflect a direct impact on granular cells or may stem from changes early in epidermal lineage progression considering that *Ovol1/2* are normally expressed in epidermal basal/spinous keratinocytes. To seek insights, we performed RNA sequencing (RNA-seq) analysis on trypsin-isolated epidermis (also contains nonepidermal cells such as LCs and dendritic epidermal T cells or DETCs) from iDKO and control littermates, followed by gene set enrichment analysis (GSEA) using single-cell RNA-seq-identified skin cell type or cell state markers (Haensel et al, 2020; Vu et al, 2022b). At 25 DPI, there was a general de-enrichment in iDKO epidermis for epidermally associated gene signatures, whereas fibroblast signature was not significantly affected (Fig 2A; Dataset EV2). By 52 DPI, iDKO epidermis was de-enriched for basal but not spinous cell marker genes and was significantly enriched for fibroblast marker genes (Fig 2B; Dataset EV2). Furthermore, iDKO epidermis showed a significant de-enrichment for marker genes of the early response (ER) or growth arrested (GA) basal cell state, but not for the *Col17a1*<sup>High</sup> or proliferative basal state (Fig 2B; Dataset EV2). These molecular alterations are consistent with *Ovol1/2* regulating epithelial-mesenchymal plasticity (i.e., suppressing fibroblast-like characteristics) and basal state transition dynamics and suggest the ER/GA basal states as likely points of deviation from a typical epithelial fate (Fig 2C). The dichotomy in basal cell state fluxes at 25 and 52 DPI may be due to *Ovol1*-specific vs. *Ovol2*-specific functions at different stages of normal epidermal differentiation.

We next sought to determine the specific molecular pathways that are impacted in iDKO epidermis. GSEA of Hallmark gene signatures revealed a de-enrichment of pathways associated with oxidative phosphorylation, adipogenesis, and fatty acid metabolism in iDKO epidermis at 25 DPI, whereas no particular pathway was enriched (Fig 2D; Appendix Fig S1A; Dataset EV2). By 52 DPI, signatures associated with EMT, cholesterol, and apical junction/surface emerged as the top enriched pathways in iDKO epidermis (Fig 2E; Dataset EV2). Several inflammation-associated gene signatures (e.g., inflammatory response, interferon gamma response, complement, and IL2-STAT signaling) were also enriched (Fig 2F; Dataset EV2). Importantly, GSEA also identified a significant enrichment of genes upregulated in psoriatic skin, but not signatures of

atopic dermatitis or ichthyosis vulgaris skin, in iDKO epidermis (Fig 2G; Dataset EV2).

Using DESeq2 with  $\geq 2$ -fold change and  $P < 0.05$  as cutoff, we identified more differentially expressed genes (DEGs) at 52 DPI compared with 25 DPI between control and iDKO epidermis (Fig 2H and I; Dataset EV3). Gene ontology (GO) analysis on the 29 upregulated DEGs at 25 DPI using Enrichr (Chen et al, 2013; Kuleshov et al, 2016; Xie et al, 2021) revealed terms related to negative regulation of I-kappaB kinase/NF-kappaB signaling (e.g., *Zc3h12a*, *Tnfrsf3*, and *Per1*), and Hsp70 protein binding (e.g., *Sacs* and *Nod2*; Appendix Fig S1B and C). While genes associated with oxidative phosphorylation (e.g., *Pdk4* and *Ndufb2*), fatty acid metabolism (e.g., *Aldh1a1* and *Hmgcs2*), and adipogenesis (e.g., *Angptl4* and *Ptger3*) did not make the stringent cutoff as downregulated DEGs, a closer examination revealed their consistent decrease in iDKO epidermis at 25 DPI (Datasets EV2 and EV4). At 52 DPI, actin binding (e.g., *Ccdc88a*, *Fscn1*, *Lcp1*, *Fxyd5*, *Iqgap2*, and *Coro1A*) and sialyltransferase activity (*St3gal4* and *St6galnac6*), both important for cell migration (Wu et al, 2018; Qi et al, 2020; Guo et al, 2021), were the top two terms enriched in the 89 upregulated DEGs in iDKO epidermis (Appendix Fig S1D). Of note, GO analysis also identified the upregulated expression of serine-type peptidase activity, specifically *Klk5/6/8*—members of the kallikrein (KLK) family of secreted serine proteases involved in regulating desquamation and inflammation (Bin et al, 2011; Kishibe, 2014; Nauroy & Nyström, 2020; Appendix Fig S1D; Dataset EV4). The top GO terms enriched for the 49 downregulated DEGs at 52 DPI included receptor ligand activity (e.g., *Bmp2/3*, *Epgn*, and *Wnt16*) and neurotrophin binding (e.g., *Ngfr* and *Ntrk2*; Appendix Fig S1E), some of which are known to be involved in epidermal fate control and keratinocyte proliferation/survival (Richardson et al, 2009; Kandyba et al, 2013; Adly et al, 2017; Mendoza-Reinoso & Beverdam, 2018; Cai et al, 2019).

Analysis of an aggregated dataset combining the 25 and 52 DPI data revealed 12 common DEGs, and 11 of them were upregulated in iDKO epidermis (Fig 2H and I; Dataset EV3). These include (i) *Zeb1*, encoding an EMT-inducing transcription factor and a known direct target of *Ovol2* repression (Watanabe et al, 2014; Lee et al, 2014a; Yang et al, 2020); (ii) genes with known association with membrane/cytoskeletal processes: *Lix1l*, *Flot2*, *Dennd5a*, *Ccdc88a*, *Cep170*, *Sacs*, and *Fez1* (Suzuki et al, 2005; Yoshimura et al, 2010; Völlner et al, 2016; Bärenz et al, 2018; Wang et al, 2018; Gentil et al, 2019; Moore et al, 2022); (iii) genes with diverse or unknown functions: *Fkbp14* (Ishikawa & Bächinger, 2014), *Zcchc24* (Cieply et al, 2016), *Klk10* (Hu et al, 2015), and *Gm4265*. The

### Figure 2. Gene expression changes in iDKO epidermis.

- A, B GSEA using top 100 marker genes of skin cell types (Vu et al, 2022b) (top) and epidermal basal cell states (Haensel et al, 2020) (bottom) at 25 or 52 DPI.  
 C Working model of epidermal differentiation trajectories in control and iDKO mice. Dashed lines indicate abnormal routes. EMP, epithelial-mesenchymal plasticity.  
 D–G GSEA using the indicated Hallmark gene pathway signatures at 25 or 52 DPI. OxPhos, oxidative phosphorylation; FA, fatty acid; IV, ichthyosis vulgaris; AD, atopic dermatitis; CP, conventional psoriasis (Ahn et al, 2018; Blunder et al, 2018).  
 H Volcano plots at 25 or 52 DPI.  
 I Venn diagrams of DEGs from separate (top) or aggregated (bottom) analyses of 25- vs. 52-DPI data. The values in parenthesis represent genes upregulated in iDKO. The 12 DEGs shared between 25 and 52 DPI are shown in the orange box (–, downregulation).  
 J RT-qPCR of the indicated genes in epidermis at 25 ( $n = 4$  biological replicates per genotype) or 52 (control:  $n = 10$  biological replicates; iDKO:  $n = 6$  biological replicates) DPI.

Data information: (J) is represented as mean  $\pm$  SD, and statistical analysis was done with the Holm–Sidak method. \* $P \leq 0.05$ ; \*\* $P \leq 0.005$ ; \*\*\* $P \leq 0.0005$ . Source data are available online for this figure.

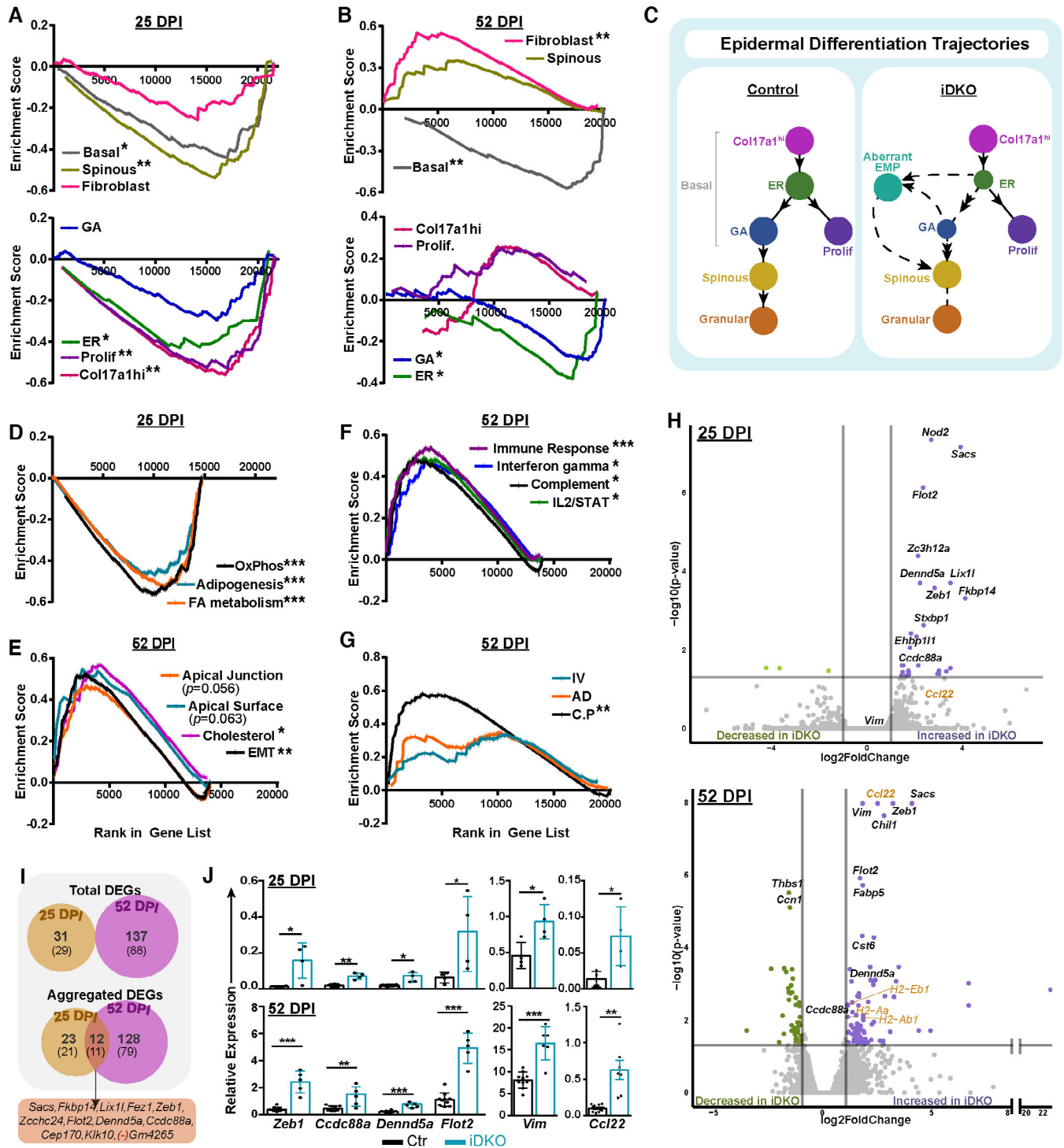


Figure 2.

upregulated expression of several *Klk* genes and their role in filaggrin processing (Sandilands *et al*, 2009; Sakabe *et al*, 2013) provide a possible basis for the expansion of filaggrin-positive zone in iDKO epidermis. *Vim*, another known *Ovol2* direct target and EMT/mesenchymal marker (Watanabe *et al*, 2014; Lee *et al*, 2014a; Haensel & Dai, 2018), was not among the identified DEGs at 25 DPI but was significantly upregulated in iDKO epidermis at 52 DPI (Fig 2H;

Dataset EV3). Similarly, immune-associated genes such as T cell chemokine *Ccl22* and major histocompatibility complex (MHC) class II genes *H2-Aa*, *H2-Ab1*, and *H2-Eb1* (Cumberbatch *et al*, 1991; Esaki *et al*, 2015) were upregulated at 52 DPI but not 25 DPI in iDKO epidermis (Fig 2H; Dataset EV3). RT-qPCR analysis of epidermal RNAs from additional pairs of control and iDKO mice confirmed the significantly elevated expression of several of these common or 52

DPI-specific genes including *Zeb1*, *Vim*, *Flot2*, *Dennd5a*, *Ccdc88a*, and *Ccl22* in iDKO epidermis at both 25 and 52 DPI (Fig 2J).

Collectively, these results corroborate our previous finding of *Ovol1/2*'s role in regulating epithelial-mesenchymal plasticity (Lee et al, 2014a), indicating that proper control of this form of plasticity is crucial in both developing and homeostatic epidermis for barrier formation and maintenance. Moreover, our analyses uncover *Ovol1/2*'s additional roles in regulating epidermal gene expression associated with metabolism and inflammation. Overall, mildly reduced metabolic gene expression emerges as early (and likely indirect given the transcriptional repressor function of *Ovol1/2*), and upregulated expression of EMT/adhesion/cytoskeleton- and immune-associated genes as late, responses to *Ovol1/2* deletion in adult epidermis.

### Identification of immune-associated genes as direct targets of *Ovo1/2* in epidermis

To elucidate the molecular mechanism of *Ovol1/2* function, we performed ChIP-seq analysis to map *Ovol1*-bound loci in adult epidermis and compared the data with our previously published *Ovol2* ChIP-seq data (Watanabe et al, 2014). A comprehensive analysis will be reported elsewhere, and here we focused on *Ovol1/2* common targets as well as immune-associated genes given the enrichment of inflammatory signatures in iDKO epidermis. We found that 697 and 849 loci were bound uniquely by *Ovol1* and *Ovol2*, respectively, whereas 361 loci were bound by both (Fig 3A; Dataset EV5). This is consistent with them having both distinct and overlapping downstream targets. Commonly targeted cellular/molecular processes include phospholipid binding, transcription coregulator activity, actin binding, tubulin binding, and microtubule binding (Fig 3B; Dataset EV6). GSEA of the 52-DPI RNA-seq data against ChIP-seq-identified targets showed that genes with elevated expression in iDKO compared with control epidermis, but not genes with reduced expression, trended toward being enriched for both *Ovol1*- and *Ovol2*-bound peaks (Fig 3C; Dataset EV7), consistent with repressor activity of *Ovol1/2* (Nair et al, 2006; Watanabe et al, 2014). Importantly, the core set of DEGs upregulated in iDKO epidermis at both 25 and 52 DPI, which include *Zeb1*, *Vim*, *Flot2*, *Dennd5a*, *Ccdc88a*, and *Ccl22*, are among the top *Ovol1/2* common targets (Figs 3D and EV2A). Moreover, *Ovol1* and *Ovol2* genes themselves are common targets (Fig EV2A), suggesting auto-regulation and cross-repression.

A closer examination revealed additional immune-associated genes, which include *Il12b*, *Il6*, *Nfkb2*, *Cx3cl1*, *Ccl27a*, and *Ccl17*, which are bound by *Ovol1* and/or *Ovol2* at weakly or strongly active promoters or adjacent enhancers per co-alignment with H3K27Ac, H3K4me1, and/or H3K4me3 histone markers (Rada-Iglesias et al, 2011; Spicuglia & Vanhille, 2012; Sethi et al, 2017; Bae & Lesch, 2020; Fig 3D; Dataset EV5). *Il12b* encodes IL-12p40, a common subunit of IL-12 and IL-23 pro-inflammatory cytokines with diverse functions (Oppmann et al, 2000; Liu et al, 2005). *Il6* encodes a barrier-associated cytokine with pleiotropic inflammatory/immune effects including LC priming and T cell responses (Cumberbatch et al, 1996; Wang et al, 2004; Tanaka et al, 2014). *Nfkb2* encodes a subunit of the NFκB complex involved in myriad inflammatory processes (Lind et al, 2008; Chawla et al, 2021). *Cx3cl1*, *Ccl27a*, and *Ccl17* encode T cell chemokines, with *Ccl17* acting as a partner of *Ccl22* in T-helper cell chemotaxis (Imai et al, 1996, 1997).

Expression of some of these genes (e.g., *Il12b*, *Il6*, *Nfkb2*, and *Cx3cl1*), although low in epidermis, was consistently increased in iDKO epidermis at 25 DPI (Fig EV2B and C; Dataset EV4). Additionally, GSEA of the Immune Pathways identified enrichment of a gene signature associated with *Nfkb2* pathway activation in iDKO epidermis 52 DPI (Fig 3E; Dataset EV2). Luminex analysis of a panel of inflammatory factors on whole skin lysates at 4–6-months post-first injection (MPI) detected significantly elevated levels of IL-12p40 and IL-6 proteins (Fig 3F). Finally, the serum level of IL-12p40 was significantly elevated in iDKO mice compared with control littermates (Fig 3G). Thus, while each inflammatory gene expression change in iDKO epidermis may be small or transient, their effects likely add up over time, producing elevated levels of secreted inflammatory factors that can enter circulation.

### Loss of *Ovol1/2* in adult epidermis triggers aberrant local immune activation during homeostasis

LCs are epidermal-resident antigen-presenting cells that maintain tolerance in homeostasis but instigate an inflammatory response after perturbation (Vulcano et al, 2001; Merad et al, 2008; Doebel et al, 2017). LCs adhere to epidermal keratinocytes, which in turn regulate LC abundance and morphology (Tang et al, 1993; Clayton et al, 2017; Park et al, 2021). The adhesion defects in iDKO epidermis led us to wonder whether LC cells are impacted. Using whole-mount immunostaining, we found LCs (langerin<sup>+</sup> or CD207<sup>+</sup>) in 52-DPI iDKO epidermis to exhibit a more rounded morphology and lack extensive dendritic projections compared with LCs in control epidermis (Fig 4A and B). Furthermore, flow cytometry revealed significantly higher mean fluorescent intensity of MHC II on LCs from iDKO epidermis compared with control counterparts, while relative abundance of LCs and DETCs remained similar (Figs 4C and D, and EV3A–C). Taken together, these data show that LCs in iDKO epidermis are in a preciously “activated” state (Nishibu et al, 2006; Kubo et al, 2009; Van den Bossche & Van Ginderachter, 2013; Redd et al, 2016; Yan et al, 2020; Yang et al, 2021).

Activated LCs are known to migrate to the regional skin-draining lymph nodes (LNs), present antigens to MHC II-restricted CD4<sup>+</sup> helper T cells and MHC I-restricted CD8<sup>+</sup> cytotoxic T cells, and recruit them to skin (Xiong & Bosselut, 2012; Clayton et al, 2017; García Nores et al, 2018). The relative abundance of CD4<sup>+</sup> T cells, albeit a small population in homeostasis, was indeed elevated in iDKO dermis compared with control dermis (Figs 4E and EV3D and E). In contrast, the abundance of total immune cells (CD45<sup>+</sup>), T cells (CD3<sup>+</sup>), immune-suppressive FoxP3<sup>+</sup> regulatory T cells (Tregs), and myeloid-derived immune cells (CD11b<sup>+</sup>F4/80<sup>-</sup> cells, macrophages, and neutrophils) was not significantly altered (Figs 4F and EV3F–L). The relative abundance of total and CD4<sup>+</sup> T cells, but not CD8<sup>+</sup> T cells, was also significantly elevated in iDKO paw skin (Figs 4G and EV3M and N). Skin-draining LNs were significantly larger in iDKO mice compared with littermate controls at 52 DPI (Fig 4H and I) and contained overall increased numbers of immune cells including LCs and T cells but with no particular skewing toward any specific T cell subset (Figs 4J–M and EV3O–Q). LN size was not different between control and iDKO mice at 15 DPI when barrier defect was first observed (Fig 4I), suggesting that blatant immune abnormalities take time to develop. Moreover, spleen weight was not affected even by 4–6 MPI (Fig EV3R), suggesting the aberrant immune activation

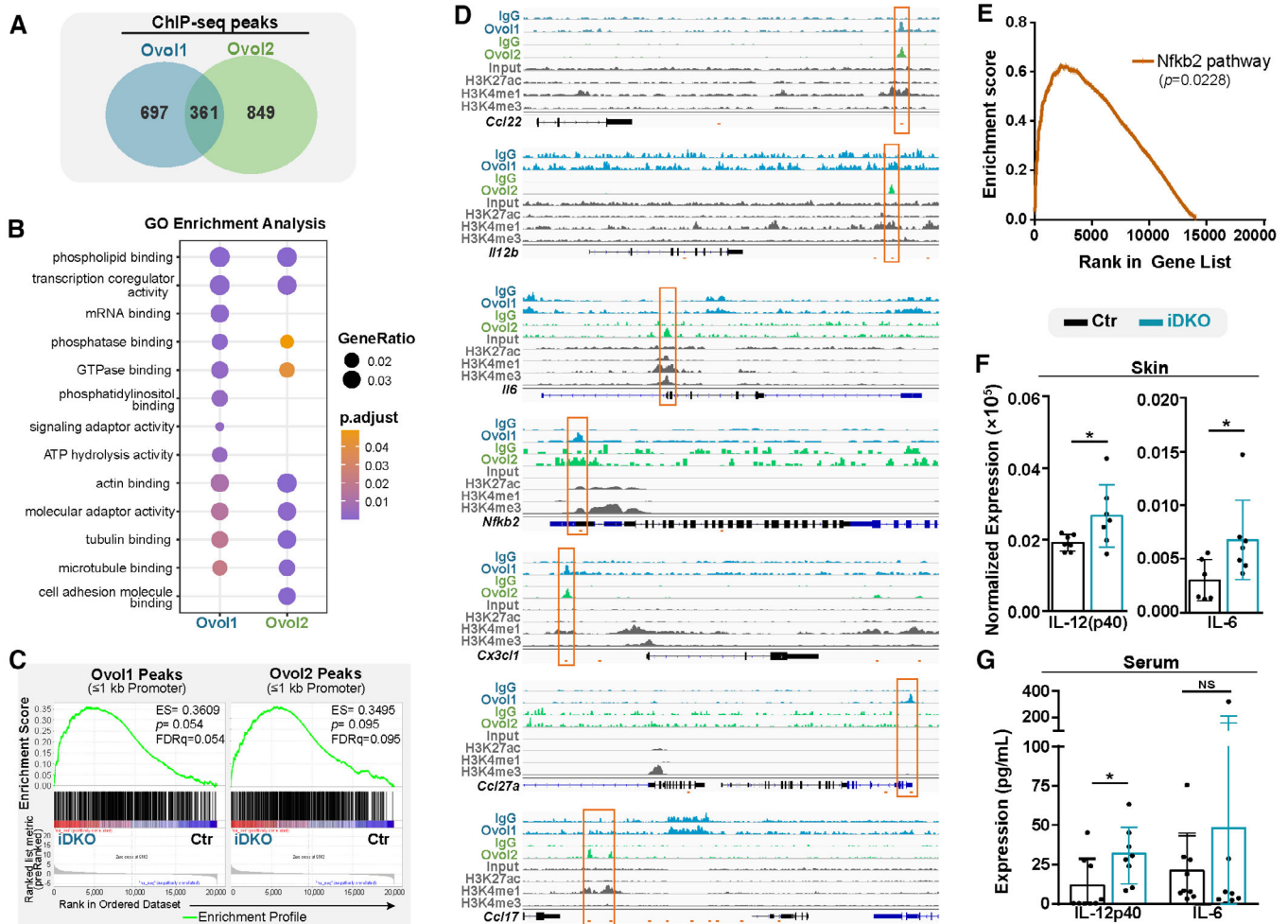


**Figure 3. Identification of Ovo1/2 direct targets.**

- A Venn diagram depicting the numbers of Ovo1- or Ovo2-specific and overlapping peaks.
- B Dot plot of GO enrichment analysis for genes that contain peaks for Ovo1 or Ovo2.
- C GSEA comparing Ovo1 or Ovo2 ChIP-seq peaks with 52-DPI RNA-seq data preranked by highest fold change enrichment in iDKO compared with control. ER, enrichment score. *P*, nominal *P*-value. FDR, FDR *q*-value.
- D ChIP-seq tracks of Ovo1, Ovo2, and histone marks for the select loci. Boxed areas indicate Ovo1/2-binding peaks, and red bars underneath indicate the presence of Ovo1/2 sequence motifs.
- E GSEA of Nfkb2 pathway signature identified by Immune SigDB at 52 DPI.
- F, G Luminex measurements of the indicated cytokines in skin lysates (F; *n* = 7 biological replicates per genotype) or serum (G; *n* = 8 biological replicates per genotype) of control and iDKO mice at 4–6 MPI.

Data information: (F, G) is represented as mean  $\pm$  SD, and statistical analysis was done with the Holm–Sidak method. NS, nonsignificant; \**P*  $\leq$  0.05. Source data are available online for this figure.

is largely confined to the local skin microenvironment. This said, a RT-qPCR screen revealed statistically significant increases in the mRNA expression of *Tnf*, *Il17f*, and *Csf3* (encoding G-CSF) in LNs from iDKO mice at this age (Fig 4N). The serum level of G-CSF, but not several other cytokines, was also increased in iDKO mice compared with control littermates (Figs 4O and EV3S and T). These results suggest that some of the inflammatory factors produced by the activated LNs in iDKO mice can enter circulation.

$\gamma\delta$ T cells are barrier-resident, LC-independent T cells important for cutaneous immunosurveillance (Sumaria et al, 2011; O'Brien & Born, 2015; Sulcova et al, 2015; Castillo-González et al, 2021). In

both back and paw skin, the relative abundance of dermal  $\gamma\delta$ T cells was significantly increased in iDKO mice compared with controls (Figs 4F and G, and EV3E, J, M, N). Increased number of  $\gamma\delta$ T cells was also observed in iDKO LNs (Figs 4M and EV3O and P). Consistent with  $\gamma\delta$ T cells being a major source of *Il17* expression (Naik & Fuchs, 2022), circulating level of IL-17 was significantly higher in iDKO mice than in control littermates at 52 DPI (Fig 4P).

Collectively, these data show that epidermal-specific loss of *Ovo1/2* in homeostatic adult skin is sufficient to trigger aberrant immune activation with both adaptive (LC/CD4<sup>+</sup> T cell/LN axis) and innate ( $\gamma\delta$ T) components.



**Ovol1/2 iDKO mice fail to accumulate body fat and exhibit altered energy metabolism**

Immune cell dysfunction and chronic inflammation can affect body weight and metabolism (Pfitzenmaier *et al*, 2003; Freigang *et al*, 2013; Bindels & Thissen, 2016; Chen *et al*, 2019). The iDKO mice offered us a useful model to examine the potential long-term, whole-body consequences of aberrant skin immune activation, especially considering that multiple inflammatory factors are elevated in circulation. Interestingly, starting at around 85 DPI (~ 4 months of age), iDKO mice exhibited a visibly smaller body

size than their control littermates (Figs 5A and B, and EV4A). Tracking body weight over time revealed that compared with control littermates, iDKO mice failed to gain weight (rather than losing weight; Fig 5C). As a control, iDKO mice that were not treated by TAM gained weight properly (Fig EV4B). By ~ 200 DPI (8 months of age), iDKO mice showed signs of premature aging (e.g., hunched stature and puffy eyes; Fig EV4A), which is in apparent correlation with an enrichment of aged skin basal cell signature (Keyes *et al*, 2016; Ge *et al*, 2020) in young iDKO epidermis (Fig EV4C). Older iDKO mice also exhibited ruffled and greasier fur compared with their littermate controls, but their hair

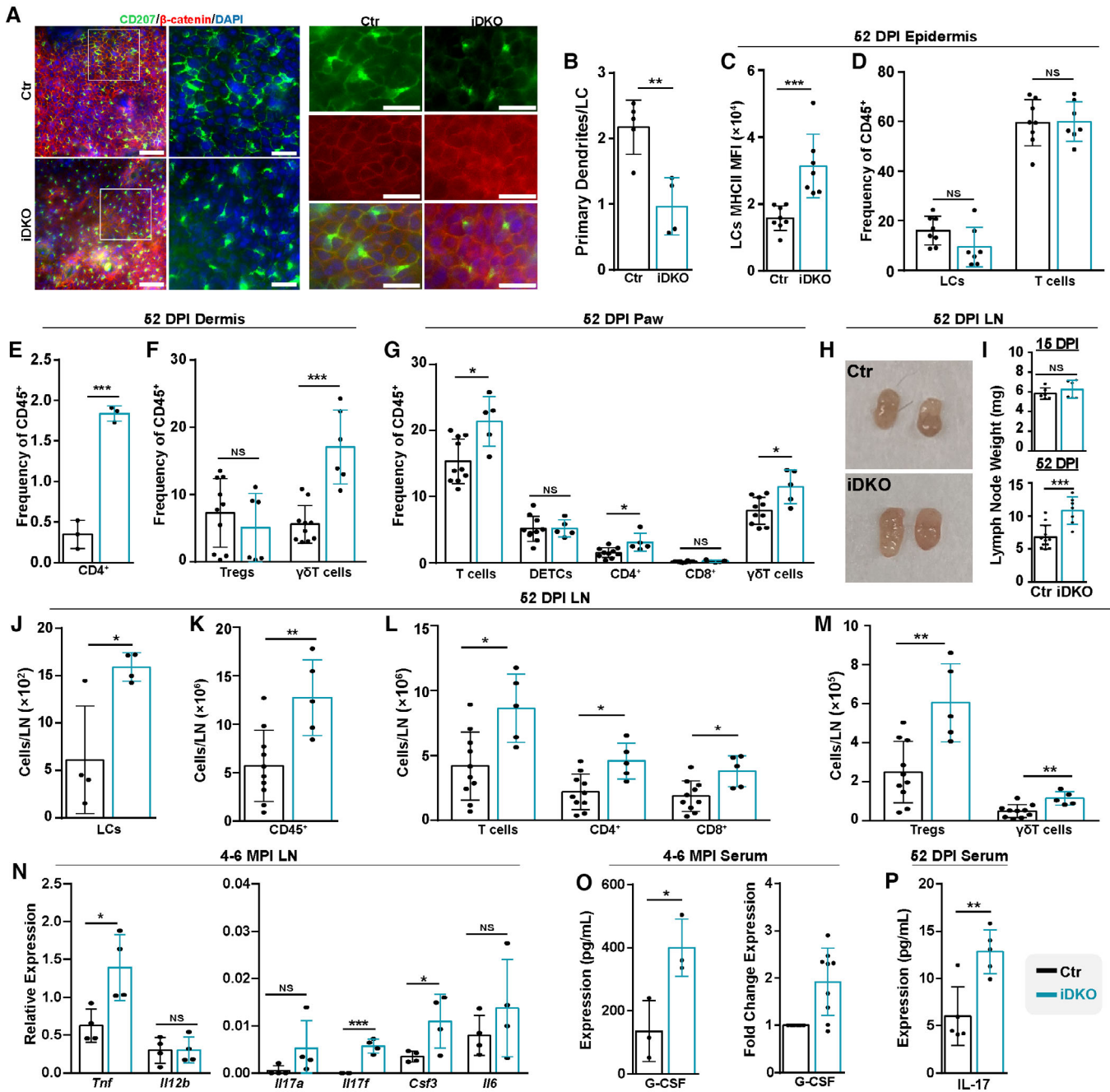


Figure 4.

**Figure 4. Evidence for aberrant immune activation in skin of iDKO mice.**

- A Representative whole-mount immunofluorescent staining of LCs in mouse back skin at 52 DPI.
- B Quantification of primary dendrites in LCs as shown in (A). Control:  $n = 5$  biological replicates; iDKO:  $n = 4$  biological replicates.
- C, D Flow cytometry analysis of isolated epidermis at 52 DPI. Control:  $n = 8$  biological replicates; iDKO:  $n = 7$  biological replicates. MFI, mean fluorescence intensity.
- E, F Flow cytometry analysis of isolated dermis at 52 DPI. Control:  $n = 4$  biological replicates; iDKO:  $n = 3$  biological replicates in (E); Control:  $n = 10$  biological replicates; iDKO:  $n = 5$  biological replicates in (F).
- G Flow cytometry analysis of paw at 52 DPI. Control:  $n = 6$  biological replicates; iDKO:  $n = 5$  biological replicates.
- H Representative images of skin-draining LNs at 52 DPI.
- I Quantification of LN weight at 15 or 52 DPI. Control:  $n = 12$  biological replicates; iDKO:  $n = 7$  biological replicates.
- J–M Flow cytometry analysis of LNs at 52 DPI.  $n = 4$  pairs for (J). Control:  $n = 10$  biological replicates; iDKO:  $n = 5$  biological replicates for (K–M).
- N RT–qPCR of the indicated genes in LNs from 4–6 MPI.  $n = 4$  biological replicates per genotype.
- O Luminex measurements of G-CSF in serum of control and iDKO mice at 4–6 MPI. Left, results obtained using remote service at Eve Technologies ( $n = 3$  biological replicates per genotype). Right, results obtained in-house using a custom panel ( $n = 8$  biological replicates per genotype).
- P Luminex measurements of IL-17 in serum of control and iDKO mice at 52 DPI.  $n = 5$  biological replicates per genotype.

Data information: Scale bars: 50  $\mu\text{m}$  (left column) and 20  $\mu\text{m}$  (three columns on the right) for (A). (B–G, I–P) is represented as mean  $\pm$  SD, and statistical analysis was done with the Holm–Sidak method. NS, nonsignificant; \* $P \leq 0.05$ ; \*\* $P \leq 0.005$ ; \*\*\* $P \leq 0.0005$ .

Source data are available online for this figure.

types, lengths, and hair cycle progression were normal (Fig EV4A and D–E).

Using Echo magnetic resonance imaging (EchoMRI) to analyze body mass composition, we detected reduced fat mass (but no change in lean mass) in iDKO mice at  $\sim 4$  MPI compared with their littermate controls (Figs 5D and EV4F; also see below). Fat reduction was widespread, affecting inguinal (i) and epididymal (e) white adipose tissues (WAT), brown adipose tissue (BAT), as well as dermal fats (dWAT; Fig 5E–G). Reduced body fat can be caused by the activation of thermogenesis in BAT (Cannon & Nedergaard, 2004; Matsushita et al, 2021). However, our RT–qPCR analysis did not detect any statistically significant increase in the expression of thermogenesis-associated genes in iDKO BAT (Fig EV4G), and there was no detectable difference in body temperature between iDKO and control mice (Fig EV4H). Analysis of iWAT revealed slightly decreased expression of thermogenesis genes *Ucp1* and *Prdm16*, but no significant change in the expression of genes involved in lipolysis (*Lipe*, *Mgl1*, and *Atgl*), fatty acid synthesis (*Fasn*), or immune modulation (e.g., *Ccl2*, *Ifng*, and *Il1a*), in iDKO mice compared with littermate controls (Fig EV4I). Interestingly, dWAT of iDKO mice showed significantly increased expression of pro-inflammatory cytokine *Tnf*, whereas changes in other inflammatory genes were not statistically significant (Fig EV4J). Overall, while iDKO mice share with some other barrier-deficient mouse models (Binczek et al, 2007; Sampath et al, 2009; Oji et al, 2010; Sano, 2015; Schmuth et al, 2015; Egawa et al, 2016; Chen et al, 2019) in showing overall body fat reduction, they do not share a detectable increase in thermogenesis.

To further define the global changes occurring in iDKO mice, we performed metabolic cage analysis both at room temperature (RT) and with cold exposure (CE) to challenge metabolic processes. At all ages examined, food intake of the iDKO mice was not significantly different from the control littermates, and movement was slightly decreased at RT at 4–5 MPI (Figs 5H–J and EV4K–M). At 2–3 MPI, there was no statistically significant difference between iDKO and control mice in energy expenditure or respiratory exchange ratio (RER; Fig EV4N and O). By 4–5 MPI, iDKO mice compared with the controls showed a significant increase in energy expenditure that persisted upon CE (Fig 5K). Furthermore, their RER was significantly higher at night than that of control littermates and the difference appeared to be exacerbated by CE (Fig 5L), suggesting a

switch in fuel utilization from fats to carbohydrates possibly as a response to low fat mass (Ramos-Jiménez et al, 2008; Speakman, 2013; Škop et al, 2020). However, no difference in serum triglyceride content was observed (Fig EV4P). Together, these results demonstrate that iDKO mice undergo whole-body metabolic adaptation to increase energy expenditure and reduce fat usage.

#### Systemic Dex treatment normalizes epidermal barrier defect, suppresses aberrant skin immune activation, and partially rescues whole-body changes in iDKO mice

Next, we performed functional experiments to investigate the potential causal relationship between aberrant skin immune activation and whole-body phenotype in iDKO mice. Given that  $\gamma\delta\text{T}$  cells represent the most abundantly enriched in iDKO skin among the immune cell types we examined, we first inhibited their function through i.p. injection of a neutralizing antibody against  $\gamma\delta\text{TCR}$  (Fig EV5A–C). The  $\gamma\delta\text{TCR}$  antibody-treated iDKO mice still showed detectable barrier dysfunction, displaying higher TEWL than that of antibody- or IgG-treated control littermates and similar to that of the IgG-treated iDKO littermates at 4 MPI (Fig EV5D). Moreover,  $\gamma\delta\text{TCR}$  blockage did not normalize the body weight and other differences between iDKO and control mice (Fig EV5E–H). These data argue against a specific role for  $\gamma\delta\text{T}$  cells in causing the weight/fat reduction of iDKO mice.

We then turned to intraperitoneally administering Dex (Fig 6A), a widely used immunosuppressant (Barshes et al, 2004; Giles et al, 2018; Lay et al, 2018). We first assessed the potential metabolic effect of Dex treatment on control mice using metabolic cage analysis. At the dosage/duration used in our experiments, Dex slightly increased body fat and reduced RER at night, but did not significantly affect body weight or energy expenditure (Fig EV5I–N).

We next systematically compared Dex responses of iDKO and control mice. Examination of the skin showed alleviation of iDKO barrier, epidermal cell rounding, and terminal differentiation defects (Figs 6B–E and EV5O and P), which is in keeping with Dex's known effect in accelerating barrier acquisition and epidermal differentiation (Patel et al, 2006). Concomitantly, the difference between iDKO and control mice in epidermal LC activation was no longer significant after Dex treatment (Fig 6F). Potent, but nonspecific immune

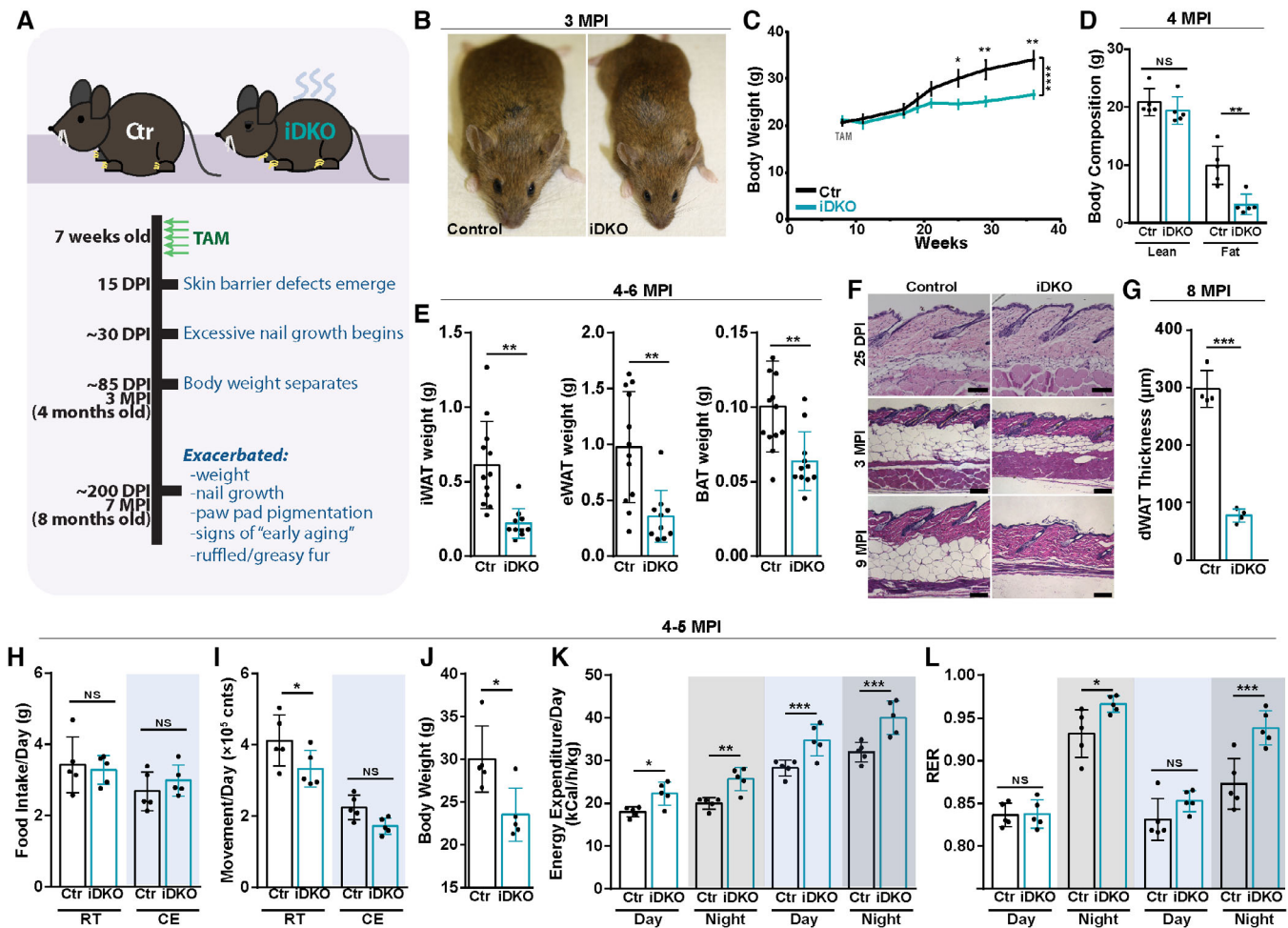


**Figure 5. Whole-body defects in iDKO mice.**

A Timeline of *Ovol1/2* iDKO phenotypes.  
 B Representative images of control and iDKO mice at 3 MPI.  
 C Body weight measurements of paired control and iDKO mice over time.  $n = 9$  biological replicates per genotype.  
 D EchoMRI measurements of body composition at 4 MPI.  $n = 5$  biological replicates per genotype.  
 E Quantification of iWAT, eWAT, and BAT tissue weight. Control:  $n = 12$  biological replicates for all subpanels; iDKO:  $n = 10$  biological replicates for iWAT and eWAT, and  $n = 11$  biological replicates for BAT.  
 F Representative H/E images of control and iDKO skin at the indicated times showing changes in dWAT.  
 G Quantification of fat cell area in (F).  $n = 4$  biological replicates per genotype.  
 H-L Results from metabolic cage analysis of 4-5-MPI control and iDKO mice ( $n = 5$  biological replicates per genotype) at RT (white band) or after CE (blue band). Gray bands designate night. Shown are data on food intake (H), movement (I), body weight (J), energy expenditure (K), and RER (L).

Data information: Scale bar: 100  $\mu\text{m}$  for (F). For (C), data are represented as mean  $\pm$  SEM and two-way ANOVA and Sidak's multiple comparisons test for individual time points were performed. For (D-E, G-L), data are represented as mean  $\pm$  SD and statistical analysis was done with the Holm-Sidak method. NS, nonsignificant; \* $P \leq 0.05$ ; \*\* $P \leq 0.005$ ; \*\*\* $P \leq 0.0005$ ; \*\*\*\* $P \leq 0.00005$ .

Source data are available online for this figure.

suppression by Dex was also evident, through drastically reducing LN size and cellular content (e.g., MHC II<sup>+</sup>/LC and T/ $\gamma\delta$ T cells) as well as reducing spleen weight in both iDKO and control mice (Figs 6G-J and EV5Q-T). Importantly, the differences between iDKO mice and control littermates in body weight and fat mass were largely abolished or significantly diminished by Dex treatment (Fig 6K and N). Taken together, these findings show that Dex administration partially normalizes the epidermal barrier and LC defects as well as the weight and fat phenotypes in iDKO mice,

providing supportive evidence that *Ovol1/2* deletion-induced epidermal and immune dysregulation at least partially contributes to the whole-body changes in weight and fat content.

## Discussion

Our study has unraveled previously unknown transcriptional regulators of adult skin barrier maintenance, as well as uncovered likely

causative links among epidermal dysregulation, local immune activation, and whole-body metabolism.

Similar to their roles in embryonic barrier development (Lee et al, 2014a), *Ovol1* and *Ovol2* suppress the aberrant expression of EMT-associated genes such as *Zeb1* and *Vim*, highlighting a shared function in regulating epithelial-mesenchymal plasticity in embryonic and adult epidermis. The overlapping molecular functions of *Ovol1* and *Ovol2* provide a mechanistic explanation for their redundant/compensatory roles in barrier development and maintenance. However, the precise roles of *Ovol1/2* in epidermal terminal differentiation remain to be better understood. Typical terminal differentiation genes, such as *Flg* whose human homolog was implicated as an *OVOL1*-responsive gene (Hirano et al, 2017; Tsuji et al, 2017), are not among the direct *Ovol1/2* targets or significantly altered genes that we identified (Dataset EV4). The upregulated *Klk* genes

in iDKO epidermis also do not contain obvious *Ovol1/2* binding sites. Instead, we surmise that the terminal differentiation defects we observed (expanded filaggrin layers but reduced barrier lipids) represent an imbalanced maturation process that originates from dysregulation of the earlier stages of epidermal lineage progression. This is not unprecedented (Bin et al, 2011) and is supported by the gene expression changes that occur in basal cells of the iDKO epidermis (Fig 2). Since *Ovol1/2* have both distinct (and even opposing) and redundant functions, the net changes in gene expression likely reflect a time-specific or differentiation state-specific balance of *Ovol1* vs. *Ovol2* function.

*OVOL1* has been previously identified as a susceptibility locus for inflammatory skin diseases such as atopic dermatitis and acne (Paternoster et al, 2011; Hirota et al, 2012; Marenholz et al, 2015), and *Ovol1* plays a protective role in psoriasis-like skin inflammation

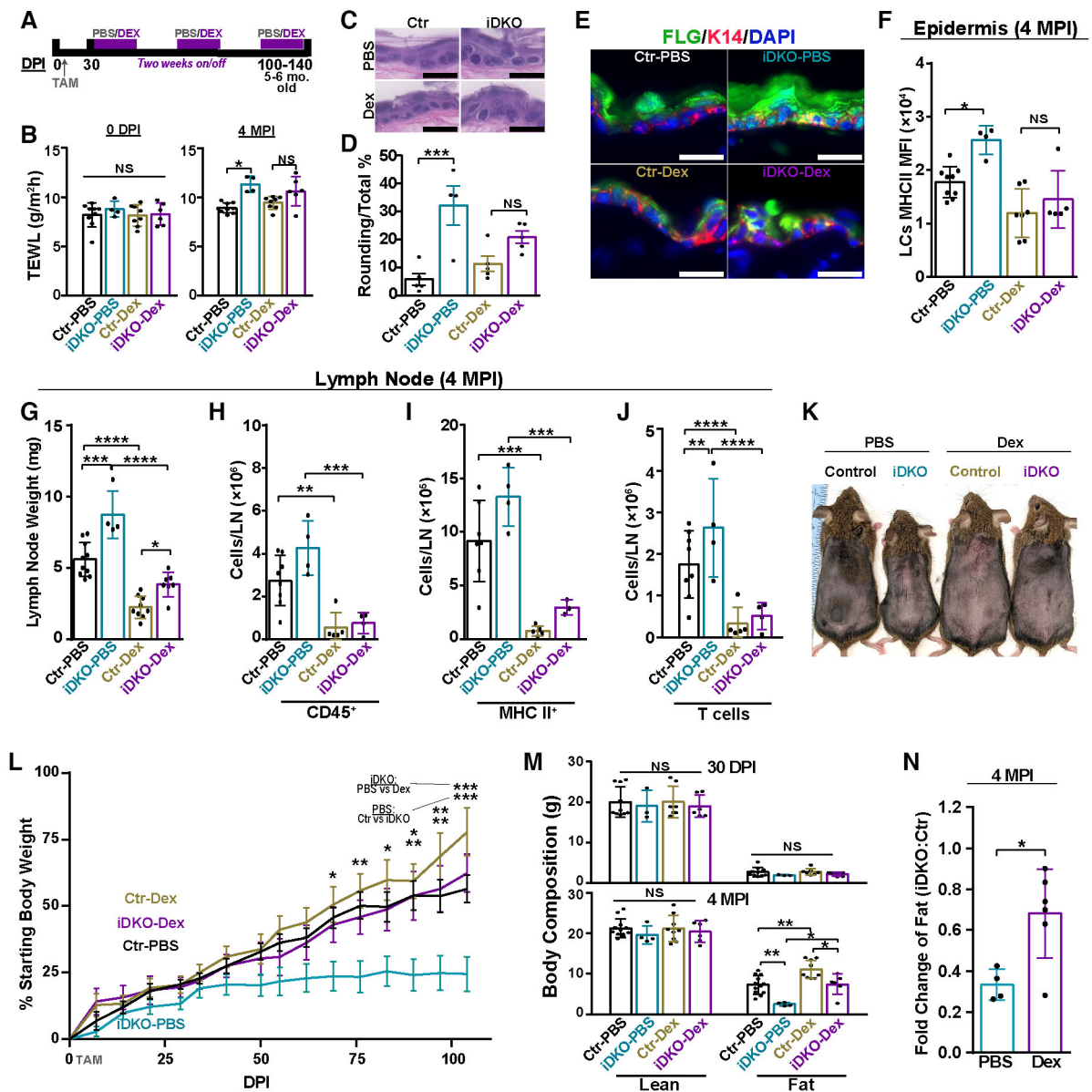


Figure 6.

**Figure 6. Dex partially rescues the skin/immune and body weight phenotypes of iDKO mice.**

- A Schematic depicting treatment strategy for Dex experiments in (B–N).
- B TEWL measurements after the indicated treatments and times. Control-PBS:  $n = 9$  biological replicates; iDKO-PBS:  $n = 4$  biological replicates; Control-Dex:  $n = 8$  biological replicates; iDKO-Dex:  $n = 6$  biological replicates.
- C, D Representative H/E images (C) and quantitative analysis (D) of epidermal cell rounding, in control and iDKO mice at 4 MPI.  $n = 4$  biological replicates for iDKO-PBS;  $n = 5$  biological replicates for all else.
- E Representative immunofluorescent images of back skin for Flg, K14, and DAPI. Quantification is shown in Fig EV50.
- F Flow cytometry analysis of epidermis at 4 MPI. Control-PBS:  $n = 9$  biological replicates; iDKO-PBS:  $n = 4$  biological replicates; Control-Dex:  $n = 7$  biological replicates; iDKO-Dex:  $n = 5$  biological replicates.
- G Quantification of LN weight. Control-PBS:  $n = 10$  biological replicates; iDKO-PBS:  $n = 4$  biological replicates; Control-Dex:  $n = 9$  biological replicates; iDKO-Dex:  $n = 7$  biological replicates.
- H–J Flow cytometry analysis of LNs at 4 MPI. Control-PBS:  $n = 8$  biological replicates; iDKO-PBS:  $n = 4$  biological replicates; Control-Dex:  $n = 5$  biological replicates; iDKO-Dex:  $n = 4$  biological replicates for (H, J) and Control-PBS:  $n = 7$  biological replicates; iDKO-PBS:  $n = 4$  biological replicates; Control-Dex:  $n = 5$  biological replicates; iDKO-Dex:  $n = 3$  biological replicates for (I).
- K Representative images of mice with the indicated treatments at 4 MPI.
- L Body weight over time represented as a percentage of the starting weight. Control-PBS:  $n = 13$  biological replicates; iDKO-PBS:  $n = 4$  biological replicates; Control-Dex:  $n = 9$  biological replicates; iDKO-Dex:  $n = 5$  biological replicates.
- M EchoMRI measurements of body composition at the indicated times. Control-PBS:  $n = 13$  biological replicates; iDKO-PBS:  $n = 4$  biological replicates; Control-Dex:  $n = 9$  biological replicates; iDKO-Dex:  $n = 6$  biological replicates.
- N iDKO/Control (Ctr) fold change in fat content at 4 MPI without and with Dex treatment, calculated from (M).

Data information: Scale bar: 20  $\mu\text{m}$  for (C, E). For (B), data are represented as mean  $\pm$  SD and statistical analysis was done using Sidak's multiple comparisons test. For (D, E, G–L), data are represented as mean  $\pm$  SD and statistical analysis was done using One-way ANOVA and Tukey's multiple comparisons test. For (B, J, L, M), data are represented as mean  $\pm$  SD and statistical analysis was done using Tukey's multiple comparisons test. NS, nonsignificant; \* $P \leq 0.05$ ; \*\* $P \leq 0.005$ ; \*\*\* $P \leq 0.0005$ ; \*\*\*\* $P \leq 0.00005$ .

Source data are available online for this figure.

(Sun *et al*, 2021). Importantly, our work identifies a number of inflammatory genes as direct targets of *Ovol1/2*, and aberrant immune activation in skin as a likely direct cellular response to *Ovol1/2* deletion in the epidermis. Based on our findings, we envision at least two possible mechanisms by which epidermal loss of *Ovol* genes alters the local skin immune microenvironment: (i) through upregulated expression of direct target genes such as *Ccl22*, *Il12b*, *Il6*, and *Nfkb2*; (ii) through precocious LC activation due to dysregulated epidermal adhesion (e.g., as a consequence of aberrant epithelial-mesenchymal plasticity; Fig 7). *IL12B* and *NFKB2* are tissue damage-associated pathways with psoriasis- and/or atopic dermatitis-associated SNPs, and both are known to expand and activate  $\gamma\delta\text{T}$  cells (Ueta *et al*, 1996; Oh & Ghosh, 2013; Mair *et al*, 2015; Braun *et al*, 2016; Yang *et al*, 2019; Manuel Sánchez-Maldonado *et al*, 2020). *IL-12* is also known to provide proliferation/survival signals to  $\text{CD4}^+$  T cells, and *Nfkb2* is important for MHC II cross-presentation (Yoo *et al*, 2002; Lind *et al*, 2008). Elevated *Il12b/IL-12p40* expression, together with precocious mobilization of LCs, are viable mechanisms underlying  $\text{CD4}^+$  T cell recruitment/expansion in skin of iDKO mice (Fig 7). Additionally, the upregulated expression of MHC II genes in iDKO epidermis, possibly as a consequence of epidermal stresses because these genes are not identified as *Ovol1/2* direct targets, can also enhance activation of  $\text{CD4}^+$  T cells (Klicznik *et al*, 2018). Together, our findings highlight a critical role of *Ovol1/2* in epidermis to orchestrate downstream molecular and cellular events that collectively maintain immune homeostasis in skin.

Our work underscores whole-body metabolic changes such as reduction of fat mass and fat utilization for energy as long-term consequences of *Ovol1/2* loss-induced epidermal dysregulation, and implicates aberrant skin immune activation as a likely causal mediator between epidermal and whole-body fat defects. Skin-specific deletion of several genes in mice has led to changes in body weight (Binczek *et al*, 2007; Sampath *et al*, 2009; Oji *et al*, 2010; Sano, 2015;

Schmuth *et al*, 2015; Egawa *et al*, 2016; Chen *et al*, 2019). For example, overexpression of *Tslp*, a cytokine involved in T helper cell 2 immune response associated with atopic dermatitis-like inflammation, protects against weight gain and fat accumulation through modulating sebum secretion (Choa *et al*, 2021). Mutation in *Gsdma3* enhances thermogenesis in BAT through epidermal secretion of *IL-6* cytokine, which is also an adipokine (Chen *et al*, 2019). *K14-Cre*-driven deletion of *Scd1* causes a reduction in body weight and fat due to lack of insulation and increased thermogenesis (Sampath *et al*, 2009). Our study not only adds *Ovol1/2* to this growing list of genetic perturbations linking epidermis with fat/whole-body defects but also uncovers *IL-17*, *IL-12p40*, and *G-CSF* as candidate molecular mediators of the systemic effects (Fig 7). Interestingly, *G-CSF* is similar to leptin in structure and downstream signaling, and exogenous *G-CSF* treatment has been shown to reduce body weight and increase energy expenditure in diabetic rats (Lee *et al*, 2014c). *IL-17* is a pro-inflammatory cytokine with complex connections to obesity and fat metabolism, one of which is to inhibit adipogenesis (Ahmed & Gaffen, 2010). *IL-6* and *TNF- $\alpha$* , two other inflammatory factors with metabolic roles (Dandona *et al*, 2004), were also enriched in the iDKO skin microenvironment although their increases in serum did not reach statistical significance. Distinct from *IL-12p40* and *IL-6*, which are direct *Ovol1/2* targets in epidermis, the enlarged LNs and abundant  $\gamma\delta\text{T}$  cells in iDKO skin are likely the major sources of *G-CSF* and *IL-17*, as a consequence of aberrant immune activation. As such, both skin and its draining LNs may contribute to the skin secretome that can potentially exert systematic effects (Caton *et al*, 2017).

We do not yet know how *Ovol1/2* deletion in epidermis causes the early, mild reduction of metabolic gene expression, because (i) *Ovol1/2* proteins are transcriptional repressors so their direct targets are expected to be upregulated in iDKO epidermis; and (ii) we were not able to identify obvious candidate metabolic regulators from our *Ovol* target screen that can link to the observed gene expression

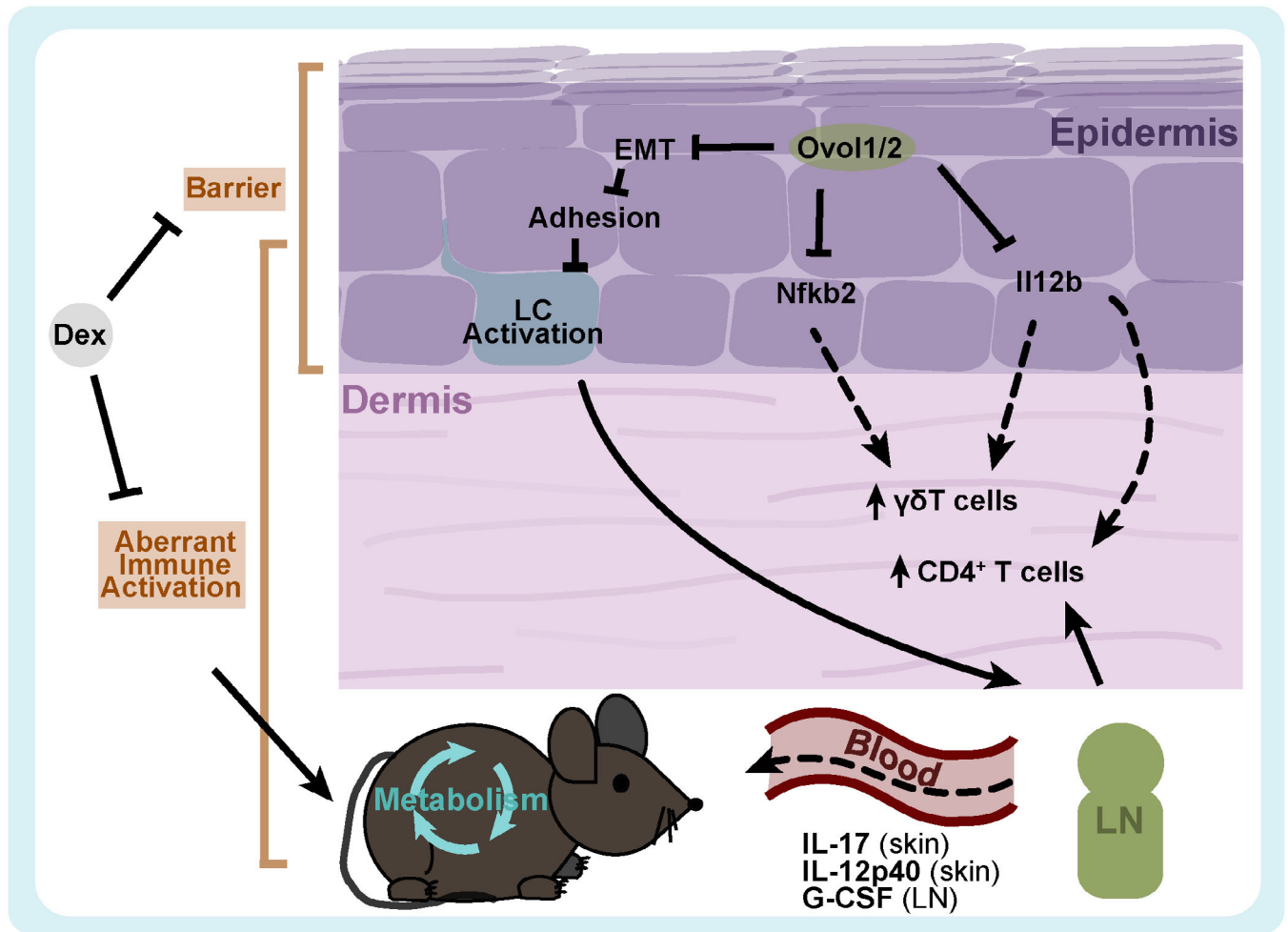


**Figure 7. Working model of mechanistic connections among *Ovov1/2* deletion-induced epidermal dysregulation, immune activation, and whole-body metabolism.**

Solid lines indicated regulations suggested by this study, whereas dashed lines indicate regulations suggested by the literature.

changes. Furthermore, jury is still out regarding whether altered metabolic gene expression in epidermis contributes to the whole-body phenotypes of iDKO mice, for example, through reduced precursor availability for adipogenesis. This is an interesting area for future exploration.

The apparent distinction of iDKO mice from the other barrier-deficient mouse models in terms of thermogenesis warrants discussion. A defective barrier would result in excessive heat and water loss. In order to sustain all metabolic functions including maintaining a stable body temperature, animals must counter heat loss through behavioral changes, mechanical insulation, or increasing the active generation of heat through metabolic reprogramming (Forni *et al.*, 2017). Similar to these other mouse models, iDKO mice showed increased energy expenditure. However, instead of increased thermogenesis as seen in the other models, our gene expression analysis of iDKO iWAT suggests the opposite. This is perhaps not surprising given the known complexity of metabolic regulations. For example, adipose tissue lipids are mobilized for energy production through lipolysis during acute inflammation and

sepsis (Sherwood *et al.*, 1970; Feingold *et al.*, 1992; Jha *et al.*, 2014), whereas catecholamine-induced lipolysis is reduced in chronic metabolic inflammation (Mowers *et al.*, 2013). Adding to this complex picture is that recently *Ovov2* has been suggested to exert a dual role in promoting BAT-mediated thermogenesis and inhibiting WAT adipogenesis to maintain energy balance (Zhang *et al.*, 2022). Therefore, it remains formally possible that *Ovov1/2* loss in epidermis reduces thermogenesis through a more direct mechanism, which opposes the barrier deficiency-induced thermogenesis. Clearly, extensive future experiments that are beyond the scope of the current work are needed to sort out the various possibilities.

Given *Ovov1/2*'s wide-ranging, but in some aspects relatively subtle, molecular functions in epidermis, we chose to ask whether Dex—a broad-acting immune suppressing glucocorticoid—can normalize the skin aberrancies in iDKO skin and assess the impact on the whole body, rather than focusing on any single putative mediating factor. Even though glucocorticoids are known to exert conflicting effects on adipogenesis and lipolysis (Campbell *et al.*, 2011; Peckett *et al.*, 2011; Lee *et al.*, 2014b), under the

condition of our experiments, Dex's most striking effect on control mice is immunosuppression. The rescue of epidermal barrier and differentiation, LC activation, as well body weight/adiposity defects in iDKO mice by Dex provides tantalizing evidence that epidermal and skin immune dysregulation might be what instigates the changes in whole-body metabolism. These findings now set the stage for exciting future work to study the endocrine function of skin and to pinpoint the definitive mechanisms and molecules by which our largest organ regulates body metabolism and physiology.

## Materials and Methods

### Mice

*Ovol1* and *Ovol2* floxed (f) alleles were previously described (Unezaki et al, 2007; Haensel et al, 2019; Dragan et al, 2022) and intercrossed to generate *Ovol1<sup>f/f</sup>*, *Ovol2<sup>f/f</sup>* breeders. *Ovol1<sup>f/f</sup>*, *Ovol2<sup>f/f</sup>* females were crossed with *Ovol1<sup>+/-</sup>*; *Ovol2<sup>+/-</sup>*; *K14-CreER* mice (Vasioukhin et al, 1999; Haensel et al, 2019; Sun et al, 2021) to generate *Ovol1<sup>f/-</sup>*; *Ovol2<sup>f/-</sup>*; *K14-CreER* (iDKO) mice that were injected with 75 mg tamoxifen/kg body weight for 5 consecutive days at 7 weeks old. All controls used are sex-matched littermates. Information for all genotyping primers is provided in Appendix Table S1. All animal studies have been approved and abide by regulatory guidelines of the Institutional Animal Care and Use Committee (IACUC) of the University of California, Irvine.

### TEWL measurements

TEWL was measured on shaved mouse back skin using the Delfin VapoMeter (SWL4400, Delfin, Kuopio, Finland) under homeostatic conditions. TEWL values were output as g/m<sup>2</sup>h.

### Histology and immunostaining

Sections from 4% paraformaldehyde-fixed, paraffin-embedded back skin were stained with H/E as described previously (Dragan et al, 2022). Sections from mouse toe were fixed in 4% paraformaldehyde for 8 h followed by decalcification in 2% paraformaldehyde/0.4 M EDTA for 2–3 weeks at 4°C followed by paraffin-embedding and staining with H/E.

For indirect immunofluorescence, mouse back skin and toe pads were trimmed and freshly frozen in optimum cutting temperature (OCT) compound (Tissue-Tek) and stained using the appropriate antibodies. The primary antibodies used were: K1, K14, and loricrin (rabbit or chicken, gifts of Julie Segre, National Institutes of Health, Bethesda, 1:1,000), Ki67 (Cell Signaling, rabbit, clone #D3B5, catalog # 9129; 1:1,000), CD207 (Fischer, 12-2075-82; Appendix Table S2). The following secondary antibodies were used: FITC-conjugated goat anti-rabbit (Vector Laboratories, FI-1000; 1:1,000), rhodamine-conjugated donkey anti-goat (Jackson ImmunoResearch Laboratories, 711-025-147; 1:1,000), rhodamine-conjugated goat anti-chicken (Jackson ImmunoResearch Laboratories, 103-295-155; 1:1,000), and Alexa Fluor 488-conjugated donkey anti-rat (ThermoFisher, A-21208; 1:1,000). Slides were mounted in Antifade medium (Vectashield H-1000; Vector

Laboratories). Images were quantified using Fiji/ImageJ software (Schindelin et al, 2012). For quantification of  $\beta$ -catenin staining,  $\geq 18$  lines were drawn through  $\sim 4$  cells/line ( $\geq 72$  cells examined per mouse) and intensity was calculated across the line. A histogram was then generated from the binned intensity values of a given mouse and averaged across all mice.

For whole-mount immunostaining, shaved back skin was stripped with adhesive cellophane tape 40 times to break the skin barrier. Stripped back skin was then removed, fat scrapped off, and the skin was cut into  $\sim 5$  mm<sup>2</sup> pieces. Skin was fixed in 4% paraformaldehyde for 1.5 h at 4°C and then incubated in 20% sucrose for 2–3 days. Immunostaining was performed using antibodies against  $\beta$ -catenin (Santa Cruz, sc-7199) and CD207 (ThermoFisher, Cat #14-2075-82; Appendix Table S2) overnight at 4°C.

### Transmission electron microscopy (TEM)

TEM was processed as reported previously (Lee et al, 2014a; Kashgari et al, 2020). Briefly, mouse back skin was isolated, trimmed and fixed in 2% paraformaldehyde and 2.5% glutaraldehyde in 0.2 M sodium cacodylate buffer, and incubated at 4°C for 2–3 days. Samples were then rinsed in 0.1 M sodium cacodylate buffer and postfixed for 2 h at room temperature in 1% aqueous osmium tetroxide in 0.1 M sodium cacodylate buffer. The samples were then dehydrated, processed, and imaged at the UC Irvine Materials Research Institute core by Dr. Li Xing.

### Tissue harvest and lipidomics

Lipids were extracted from trypsin-isolated back skin epidermis. Epidermis was snap frozen utilizing liquid nitrogen precooled Wollenberger clamp (PMID: 13845757). Tissues were grinded into powder using a Cryomill (Retsch, Newtown, PA). Powder was weighed ( $\sim 20$  mg) on dry ice and isopropanol added at 40 $\times$  the weight of the tissue powder to make a mixture solution of 25 mg of tissue/mL of solvent, vortexed, and centrifuged at 16,000 g for 10 min at 4°C. Three  $\mu$ Ls of supernatant were used for liquid chromatography–mass spectrometry analysis (LC–MS). For LC–MS, samples were analyzed via quadrupole-orbitrap mass spectrometer (Q Exactive Plus, Thermo Fisher Scientific, San Jose, CA), operating in a positive ion mode via electrospray ionization coupled to Atlantis T3 Column (150  $\times$  2.1 mm, 3  $\mu$ m particle size; Waters, Milford, MA) to scan from mass/charge ratio 290 to 1,200 and 140,000 resolution. LC separation was conducted at 45°C using a gradient of solvent A (10% methanol in water 1 mM ammonium acetate and 35 mM acetic acid) and solvent B (98% isopropanol and 2% methanol with 1 mM ammonium acetate and 35 mM acetic acid). Flow rate was 150  $\mu$ L/min. The LC gradient was as follows: 0 min, 25% B; 2 min, 25% B; 5.5 min, 65% B; 12.5 min, 100% B; 16.5 min, 100% B; 17 min, 25% B; and 30 min, 25% B. Autosampler temperature was set at 4°C. Data were analyzed using the MAVEN software and Compound Discoverer software (Thermo Fisher Scientific, San Jose, CA).

### RT-qPCR and RNA-seq

Tissues were collected ad libitum for gene expression analysis. iWAT, BAT, dWAT, and single-cell suspension of epidermis (see

below) were homogenized in Trizol (ThermoFisher, 15596018), followed by chloroform extraction and RNA purification from the aqueous phase using ZYMO RESEARCH Quick-RNA MiniPrep per manufacturer's protocol. RNA was quantified using the NanoDrop ND-1000 spectrophotometer (ThermoFisher) and quality checked using the Agilent Bioanalyzer 2100 (Agilent). For RT-PCR, 2 µg of RNA was used to generate cDNA (Applied Biosystems, 4368814) per manufacturer's protocol. qPCR was performed using a Bio-Rad CFX96 Real-Time System and SsoAdvanced Universal SYBR® Green Supermix (Bio-Rad, 172-5271). *Gapdh* was used as a loading control. Information for gene-specific primers used is provided in Appendix Table S3.

Library construction was performed according to the Illumina TruSeq® Stranded mRNA Sample Preparation Guide. One µg of total RNA was used, and mRNA was enriched using oligo dT magnetic beads. The enriched mRNA was chemically fragmented for 3 min, followed by reverse transcription to make cDNA. The resulting cDNA was cleaned using AMPure XP beads, end repaired, and the 3' ends were adenylated. Illumina barcoded adapters were ligated on the ends, and the adapter-ligated fragments were enriched by 9 cycles of PCR. The resulting libraries were validated by qPCR and sized by Agilent Bioanalyzer DNA high-sensitivity chip. The barcoded cDNA libraries were multiplexed on the Illumina HiSeq 4000 platform to yield 100-bp paired-end reads. FASTQ files were trimmed using Trimmomatic version 0.35 (Bolger et al, 2014a) and aligned to the mm10 genome and counted using STAR version 2.5.2a (Dobin et al, 2013). Differential expression analysis was performed using DESeq2 version 1.24.0 (Love et al, 2014) on R version 3.6.1.

### ChIP-seq

ChIP-seq analysis was performed on skin harvested at 6 h after imiquimod treatment, such that the level of *Ovol1* protein expression was sufficiently high to enable success (Dragan et al, 2022). To separate epidermis from dermis, back skin was collected and digested with 0.25% trypsin for 1 h at 37°C, scraped, minced, resuspended in 5% fetal bovine serum in PBS, and filtered through 70-µm and then 40-µm filters. Epidermal cells in single-cell suspension were then cross-linked in 1% formaldehyde, followed by ChIP assay using rabbit anti-*Ovol1* antibody (Dai et al, 1998) and SimpleChIP® Enzymatic Chromatin IP Kit Magnetic Beads (9006, Cell Signaling) according to the manufacturer's instructions. DNA was then purified and NexteraPE adapters were ligated on the ends and the adapter-ligated fragments were enriched by 9 cycles of PCR. The resulting libraries were validated by Agilent Bioanalyzer dsDNA high-sensitivity chip. The barcoded DNA libraries were multiplexed on the Illumina HiSeq 4000 platform to yield 100-bp paired-end reads. FASTQ files were trimmed using Trimmomatic version 0.35 (Bolger et al, 2014a), aligned to the mm10 genome using Bowtie2 version 2.2.3 (Langmead & Salzberg, 2012), and sorted/removed duplicates using Samtools version 1.3 (Danecek et al, 2021) and Picard tools version 1.87 (<http://broadinstitute.github.io/picard>). Finally, peaks were called with MACS2 (Zhang et al, 2008).

### Flow cytometry

Back skin, paw skin (removed from bone), and LNs were dissected. LNs were crushed in FACS buffer (5% fetal bovine serum in 1xPBS),

filtered through a 70-µm filter, rinsed, and resuspended in FACS buffer.

Epidermis and dermis were separated using incubation with 0.25% trypsin (Sigma; T4799) for 30 min to 1.5 h at 37°C. Epidermis was minced, filtered through a 40-µm filter, rinsed, and resuspended in FACS buffer. Minced dermis and whole paw skin were digested with 10 ml of a solution containing 0.25% collagenase (Sigma, C9091), 0.01 M HEPES (ThermoFisher, BP310), 0.001 M sodium pyruvate (ThermoFisher, BP356), and 0.1 mg/mL DNase (Sigma, DN25) at 37°C for 30 min (dermis) or 1 h (paw) with rotation, and then filtered through a 40-µm filter, spun down, and resuspended in FACS buffer. Cells were stained by incubation for 30 min on ice with the antibodies listed in Appendix Table S2.

### Luminex and triglyceride assays

Either serum or flash-frozen whole skin in RIPA buffer (Dragan et al, 2022) was used for analysis. For cytokine protein measurements, a custom-made cytokine/chemokine kit (Millipore Sigma, MCYTOMAG-70K-08C) including (IL-12 p40, IL-17A, IL-1 $\alpha$ , IL-1 $\beta$ , IL-6, CXCL1, TNF- $\alpha$ , and G-CSF) was used following the manufacturer's protocol and measured on Luminex except for when noted in the relevant figure legends. Standard curves were generated using 5-parameter logistic regression, and differences in analyte levels between control and knockout samples. Cytokine values for whole skin were normalized to total protein levels measured using the Pierce™ BCA Protein Assay Kit (Thermo Scientific, 23227). Serum triglyceride levels were measured using a triglyceride assay kit (Abcam, AB65336) per the manufacturer's protocol.

### Indirect calorimetry and EchoMRI

Oxygen consumption (ml/h), carbon dioxide release (ml/h), RER, locomotor activity (counts), and food intake (grams) were monitored for individually housed mice using the Phenomaster metabolic cages (TSE Systems Inc., Chesterfield, MO). The climate chamber was set to 21°C, 50% humidity with a 12-h light–dark cycle as the home cage environment. Animals were entrained for 2 days in the metabolic cages before the start of each experiment to allow for environmental acclimation. For CE experiments, the temperature was set to rapidly drop to 4°C starting when the light cycle turned on post acclimation and RT measurements. Data were collected at 40-min intervals, and each cage was recorded for 3.25 min before time point collection.

Body composition was measured using EchoMRI™ Whole Body Composition Analyzer (Houston, TX), which provides whole body fat and lean mass measurements.

### In vivo administration of Dex and anti- $\gamma\delta$ TCR antibody

For Dex experiments, same-sex/same-weight control and iDKO littermates were intraperitoneally injected with either PBS or 1 mg Dex (in PBS) per kg body weight for 14 days on and off starting at 30 DPI and ending at 4–5 MPI. For  $\gamma\delta$ TCR blocking (Koenecke et al, 2009)/depletion (Sandrock et al, 2018) experiments, same-sex/same-weight control and iDKO mice were intraperitoneally injected with 0.5 mg of hamster anti-mouse TCR  $\gamma/\delta$  antibody (UC7-



13D5, Biolegend) or hamster IgG control (HTK888, Biolegend) on 30 DPI and then 0.2 mg every 3 days starting at 31 DPI and ending at 4 MPI. Mouse tissue samples were then collected for either flow cytometry or histology.

### Statistics and reproducibility

Most experiments were performed at least twice and on three biological replicates as indicated in the relevant figure legends. No data were excluded. Information on specific statistical methods in Prism used for analysis is also described in figure legends. For bulk RNA-seq analysis, adjusted *P*-value were generated using the negative binomial generalized models and Wald test employed by DESeq2. *P*-values  $\leq 0.05$  were considered statistically significant.

### Data availability

Datasets generated for this article are deposited in the GEO database under accession code GSE211894 (<https://www.ncbi.nlm.nih.gov/geo/query/acc.cgi?acc=GSE211894>). The accession code for previously published Ovol2 ChIP-seq data is GSE54126 (<https://www.ncbi.nlm.nih.gov/geo/query/acc.cgi?acc=GSE54126>).

**Expanded View** for this article is available [online](#).

### Acknowledgements

We thank Bogi Andersen for the use of Vapometer, Bruce Blomberg for the use of EchoMRI, Qing-Sheng Mi for advice on LCs, Max Plikus for advice on toe processing, and Nam Nguyen for advice on bioinformatics. We also thank the Genomics Research and Technology Hub, the Institute for Immunology FACS Core Facility, and Center for Transmission Electron Microscopy Facility at the University of California, Irvine (UCI) for expert service. This work was supported by NIH Grants R01-AR068074, R35-GM145307, R01-GM123731, UCI Office of Research (X.D.), and a seed grant from UCI Skin Biology Resource-Based Center (P30-AR075047; S.M. and X.D.). M.D. is partially supported by the NIH T32 Immunology Research Training Grant (AI 060573) and is a predoctoral fellow in NSF-Simons Center for Multiscale Cell Fate Research supported through NSF grant (DMS-1763272) and Simons Foundation grant (594598; Q.N.).

### Author contributions

**Morgan Dragan:** Data curation; formal analysis; validation; investigation; visualization; methodology; writing – original draft; writing – review and editing. **Zeyu Chen:** Investigation; methodology. **Yumei Li:** Data curation; formal analysis. **Johnny Le:** Data curation; formal analysis; investigation. **Peng Sun:** Investigation; visualization. **Daniel Haensel:** Investigation. **Suhas Sureshchandra:** Investigation. **Anh Pham:** Investigation. **Eddie Lu:** Investigation. **Katherine, Thanh Pham:** Investigation. **Amandine, C Verlande:** Investigation. **Remy Vu:** Investigation. **Guadalupe Gutierrez:** Investigation. **Wei Li:** Supervision; methodology. **Cholsoo Jang:** Supervision; methodology; writing – review and editing. **Selma Masri:** Supervision; methodology; writing – review and editing. **Xing Dai:** Conceptualization; resources; supervision; funding acquisition; methodology; writing – original draft; project administration; writing – review and editing.

### Disclosure and competing interests statement

The authors declare that they have no conflict of interest.

## References

- Adly MA, Assaf H, Hussein MR (2017) Neurotrophins and skin aging. In *Textbook of aging skin*, Farage MA, Miller KW, Maibach HI (eds), pp 515–527. Berlin/Heidelberg: Springer
- Ahmed M, Gaffen SL (2010) IL-17 in obesity and adipogenesis. *Cytokine Growth Factor Rev* 21: 449–453
- Ahn R, Yan D, Chang HW, Lee K, Bhattarai S, Huang ZM, Nakamura M, Singh R, Affi L, Taravati K et al (2018) RNA-seq and flow-cytometry of conventional, scalp, and palmoplantar psoriasis reveal shared and distinct molecular pathways. *Sci Rep* 8: 11368
- Bae S, Lesch BJ (2020) H3K4me1 distribution predicts transcription state and poising at promoters. *Front Cell Dev Biol* 8: 289
- Bärenz F, Kschonsak YT, Meyer A, Jafarpour A, Lorenz H, Hoffmann I (2018) Ccdc61 controls centrosomal localization of Cep170 and is required for spindle assembly and symmetry. *Mol Biol Cell* 29: 3105–3118
- Barshes NR, Goodpastor SE, Goss JA (2004) Pharmacologic immunosuppression. *Front Biosci* 9: 411–420
- Bin L, Kim BE, Hall CF, Leach SM, Leung DYM (2011) Inhibition of transcription factor specificity protein 1 alters the gene expression profile of keratinocytes leading to upregulation of kallikrein-related peptidases and thymic stromal lymphopoietin. *J Invest Dermatol* 131: 2213–2222
- Binczek E, Jenke B, Holz B, Günter RH, Thevis M, Stoffel W (2007) Obesity resistance of the stearoyl-CoA desaturase-deficient (scd1  $-/-$ ) mouse results from disruption of the epidermal lipid barrier and adaptive thermoregulation. *Biol Chem* 388: 405–418
- Bindels LB, Thissen JP (2016) Nutrition in cancer patients with cachexia: a role for the gut microbiota? *Clin Nutr Exp* 6: 74–82
- Blunder S, Köks S, Köks G, Reimann E, Hackl H, Gruber R, Moosbrugger-Martinz V, Schmuth M, Dubrac S (2018) Enhanced expression of genes related to xenobiotic metabolism in the skin of patients with atopic dermatitis but not with ichthyosis vulgaris. *J Invest Dermatol* 138: 98–108
- Bolger AM, Lohse M, Usadel B (2014) Trimmomatic: a flexible trimmer for Illumina sequence data. *Bioinformatics* 30: 2114–2120
- Braun M, Ress ML, Yoo YE, Scholz CJ, Eyrcir M, Schlegel PG, Wölfel M (2016) IL12-mediated sensitizing of T-cell receptor-dependent and -independent tumor cell killing. *Oncimmunology* 5: e1188245
- Brunner PM, Guttman-Yassky E, Leung DY (2017) The immunology of atopic dermatitis and its reversibility with broad-spectrum and targeted therapies. *J Allergy Clin Immunol* 139: S65–S76
- Cai B, Zheng Y, Yan J, Wang J, Liu X, Yin G (2019) BMP2-mediated PTEN enhancement promotes differentiation of hair follicle stem cells by inducing autophagy. *Exp Cell Res* 385: 111647
- Campbell JE, Peckett AJ, D'Souza AM, Hawke TJ, Riddell MC (2011) Adipogenic and lipolytic effects of chronic glucocorticoid exposure. *Am J Physiol Cell Physiol* 300: 198–209
- Cannon B, Nedergaard J (2004) Brown adipose tissue: function and physiological significance. *Physiol Rev* 84: 277–359
- Castillo-González R, Cibrian D, Sánchez-Madrid F (2021) Dissecting the complexity of  $\gamma\delta$  T-cell subsets in skin homeostasis, inflammation, and malignancy. *J Allergy Clin Immunol* 147: 2030–2042
- Caton PW, Evans EA, Philpott MP, Hannen RF (2017) Can the skin make you fat? A role for the skin in regulating adipose tissue function and whole-body glucose and lipid homeostasis. *Curr Opin Pharmacol* 37: 59–64
- Chambers ES, Vukmanovic-Stejic M (2020) Skin barrier immunity and ageing. *Immunology* 160: 116–125
- Chawla M, Mukherjee T, Deka A, Chatterjee B, Sarkar UA, Singh AK, Kedia S, Lum J, Dhillon MK, Banoth B et al (2021) An epithelial Nfkb2 pathway

- exacerbates intestinal inflammation by supplementing latent RelA dimers to the canonical NF- $\kappa$ B module. *Proc Natl Acad Sci USA* 118: e2024828118
- Chen EY, Tan CM, Kou Y, Duan Q, Wang Z, Meirelles GV, Clark NR, Ma'ayan A (2013) Enrichr: interactive and collaborative HTML5 gene list enrichment analysis tool. *BMC Bioinformatics* 14: 128
- Chen Q, Shi P, Wang D, Liu Q, Li X, Wang Y, Zou D, Huang Z, Gao X, Lin Z (2019) Epidermis-activated Gasdermin-A3 enhances thermogenesis of Brown adipose tissue through IL-6/Stat3 signaling. *Am J Pathol* 189: 1041–1052
- Choa R, Tohyama J, Wada S, Meng H, Hu J, Okumura M, May RM, Robertson TF, Langan Pai RA, Nace A et al (2021) Thymic stromal lymphopoietin induces adipose loss through sebum hypersecretion. *Science* 373: eabd2893
- Choi MJ, Maibach HI (2005) Role of ceramides in barrier function of healthy and diseased skin. *Am J Clin Dermatol* 6: 215–223
- Cieply B, Park JW, Nakauka-Ddamba A, Bebee TW, Guo Y, Shang X, Lengner CJ, Xing Y, Carstens RP (2016) Multiphasic and dynamic changes in alternative splicing during induction of pluripotency are coordinated by numerous RNA-binding proteins. *Cell Rep* 15: 247–255
- Clayton K, Vallejo AF, Davies J, Sirvent S, Polak ME (2017) Langerhans cells-programmed by the epidermis. *Front Immunol* 8: 1676
- Coderch L, López O, De La Maza A, Parra JL (2003) Ceramides and skin function. *Am J Clin Dermatol* 4: 107–129
- Cumberbatch M, Gould SJ, Peters SW, Kimber I (1991) MHC class II expression by Langerhans' cells and lymph node dendritic cells: possible evidence for maturation of Langerhans' cells following contact sensitization. *Immunology* 74: 414–419
- Cumberbatch M, Dearman RJ, Kimber I (1996) Constitutive and inducible expression of interleukin-6 by Langerhans cells and lymph node dendritic cells. *Immunology* 87: 513–518
- Dai X, Schonbaum C, Degenstein L, Bai W, Mahowald A, Fuchs E (1998) The ovo gene required for cuticle formation and oogenesis in flies is involved in hair formation and spermatogenesis in mice. *Genes Dev* 12: 3452–3463
- Dainichi T, Kitoh A, Otsuka A, Nakajima S, Nomura T, Kaplan DH, Kabashima K (2018) The epithelial immune microenvironment (EIME) in atopic dermatitis and psoriasis. *Nat Immunol* 19: 1286–1298
- Dandona P, Aljada A, Bandyopadhyay A (2004) Inflammation: the link between insulin resistance, obesity and diabetes. *Trends Immunol* 25: 4–7
- Danecek P, Bonfield JK, Liddle J, Marshall J, Ohan V, Pollard MO, Whitwham A, Keane T, McCarthy SA, Davies RM et al (2021) Twelve years of SAMtools and BCFtools. *Gigascience* 10: giab008
- Dereksson K, Kjartansson S, Hjartardóttir H, Arngrimsson R (2012) Rare disease: ichthyosis prematurity syndrome with separation of fetal membranes and neonatal asphyxia. *BMJ Case Rep* 2012: <https://doi.org/10.1136/bcr.02.2012.5823>
- Dobin A, Davis CA, Schlesinger F, Drenkow J, Zaleski C, Jha S, Batut P, Chaisson M, Gingeras TR (2013) STAR: ultrafast universal RNA-seq aligner. *Bioinformatics* 29: 15–21
- Doebel T, Voisin B, Nagao K (2017) Langerhans cells – the macrophage in dendritic cell clothing. *Trends Immunol* 38: 817–828
- Dragan M, Sun P, Chen Z, Ma X, Vu R, Shi Y, Villalta SA, Dai X (2022) Epidermis-intrinsic transcription factor Ovol1 coordinately regulates barrier maintenance and neutrophil accumulation in psoriasis-like inflammation. *J Invest Dermatol* 142: 583–593.e5
- Egawa G, Kabashima K, Saitama K, Japan S (2016) Multifactorial skin barrier deficiency and atopic dermatitis: essential topics to prevent the atopic march. *J Allergy Clin Immunol* 138: 350–358.e1
- Elias PM (2007) The skin barrier as an innate immune element. *Semin Immunopathol* 29: 3–14
- Elias PM, Wakefield JS (2014) Mechanisms of abnormal lamellar body secretion and the dysfunctional skin barrier in patients with atopic dermatitis. *J Allergy Clin Immunol* 134: 781–791.e1
- Elias PM, Williams ML, Feingold KR (2012) Abnormal barrier function in the pathogenesis of ichthyosis: therapeutic implications for lipid metabolic disorders. *Clin Dermatol* 30: 311–322
- Esaki H, Ewald DA, Ungar B, Rozenblit M, Zheng X, Xu H, Estrada YD, Peng X, Mitsui H, Litman T et al (2015) Identification of novel immune and barrier genes in atopic dermatitis by means of laser capture microdissection. *J Allergy Clin Immunol* 135: 153–163
- Feingold KR, Doerrler W, Dinarello CA, Fiers W, Grunfeld C (1992) Stimulation of lipolysis in cultured fat cells by tumor necrosis factor, interleukin-1, and the interferons is blocked by inhibition of prostaglandin synthesis. *Endocrinology* 130: 10–16
- Fluhr JW, Elias PM, Man MQ, Hupe M, Selden C, Sundberg JP, Tschachler E, Eckhart L, Mauro TM, Feingold KR (2010) Is the Filaggrin–histidine–Urocanic acid pathway essential for stratum Corneum acidification? *J Invest Dermatol* 130: 2141–2144
- Forni MF, Peggolia J, Braga TT, Chinchilla JEO, Shinohara J, Navas CA, Camara NOS, Kowaltowski AJ (2017) Caloric restriction promotes structural and metabolic changes in the skin. *Cell Rep* 20: 2678–2692
- Freigang S, Ampenberger F, Weiss A, Kanneganti TD, Iwakura Y, Hersberger M, Kopf M (2013) Fatty acid-induced mitochondrial uncoupling elicits inflammasome-independent IL-1 $\alpha$  and sterile vascular inflammation in atherosclerosis. *Nat Immunol* 14: 1045–1053
- Gabay C, Kushner I (1999) Acute-phase proteins and other systemic responses to inflammation. *N Engl J Med* 340: 448–454
- García Nores GD, Ly CL, Cuzzone DA, Kataru RP, Hespe GE, Torrisi JS, Huang JJ, Gardenier JC, Savetsky IL, Nitti MD et al (2018) CD4+ T cells are activated in regional lymph nodes and migrate to skin to initiate lymphedema. *Nat Commun* 9: 1970
- Ge Y, Miao Y, Gur-Cohen S, Gomez N, Yang H, Nikolova M, Polak L, Hu Y, Verma A, Elemento O et al (2020) The aging skin microenvironment dictates stem cell behavior. *Proc Natl Acad Sci USA* 117: 5339–5350
- Gentil BJ, Lai GT, Menade M, Larivière R, Minotti S, Gehring K, Chapple JP, Brais B, Durham HD (2019) Sacsin, mutated in the ataxia ARSACS, regulates intermediate filament assembly and dynamics. *FASEB J* 33: 2982–2994
- Giles AJ, Hutchinson MKND, Sonnemann HM, Jung J, Fecci PE, Ratnam NM, Zhang W, Song H, Bailey R, Davis D et al (2018) Dexamethasone-induced immunosuppression: mechanisms and implications for immunotherapy. *J Immunother Cancer* 6: 51
- Guo Y, Zhang X, Wang L, Li M, Shen M, Zhou Z, Zhu S, Li K, Fang Z, Yan B et al (2021) The plasma exosomal miR-1180-3p serves as a novel potential diagnostic marker for cutaneous melanoma. *Cancer Cell Int* 21: 487
- Haensel D, Dai X (2018) Epithelial-to-mesenchymal transition in cutaneous wound healing: where we are and where we are heading. *Dev Dyn* 247: 473–480
- Haensel D, Sun P, MacLean AL, Ma X, Zhou Y, Stemmler MP, Brabletz S, Bex G, Plikus MV, Nie Q et al (2019) An Ovol2-Zeb1 transcriptional circuit regulates epithelial directional migration and proliferation. *EMBO Rep* 20: e46273
- Haensel D, Jin S, Sun P, Cinco R, Dragan M, Nguyen Q, Cang Z, Gong Y, Vu R, MacLean AL et al (2020) Defining epidermal basal cell states during skin homeostasis and wound healing using single-cell transcriptomics. *Cell Rep* 30: 3932–3947.e6
- Hardman MJ, Sisi P, Banbury DN, Byrne C (1998) Patterned acquisition of skin barrier function during development. *Development* 125: 1541–1552
- Henneke P, Kierdorf K, Hall LJ, Sperandio M, Hornef M (2021) Perinatal development of innate immune topology. *Elife* 10: e67793

- Hirano A, Goto M, Mitsui T, Hashimoto-Hachiya A, Tsuji G, Furue M (2017) Antioxidant artemisia princeps extract enhances the expression of filaggrin and loricrin via the AHR/OVOL1 pathway. *Int J Mol Sci* 18: 1948
- Hirota T, Takahashi A, Kubo M, Tsunoda T, Tomita K, Sakashita M, Yamada T, Fujieda S, Tanaka S, Doi S et al (2012) Genome-wide association study identifies eight new susceptibility loci for atopic dermatitis in the Japanese population. *Nat Genet* 44: 1222–1226
- Hooper JK, Eggink LL (2022) The discovery and function of Filaggrin. *Int J Mol Sci* 23: 1455
- Hu J, Lei H, Fei X, Liang S, Xu H, Qin D, Wang Y, Wu Y, Li B (2015) NES1/KLK10 gene represses proliferation, enhances apoptosis and down-regulates glucose metabolism of PC3 prostate cancer cells. *Sci Rep* 5: 17426
- Imai T, Yoshida T, Baba M, Nishimura M, Kakizaki M, Yoshie O (1996) Molecular cloning of a novel T cell-directed CC chemokine expressed in thymus by signal sequence trap using Epstein-Barr virus vector. *J Biol Chem* 271: 21514–21521
- Imai T, Baba M, Nishimura M, Kakizaki M, Takagi S, Yoshie O (1997) The T cell-directed CC chemokine TARC is a highly specific biological ligand for CC chemokine receptor 4. *J Biol Chem* 272: 15036–15042
- Ishikawa Y, Bächinger HP (2014) A substrate preference for the rough endoplasmic reticulum resident protein FKBP22 during collagen biosynthesis. *J Biol Chem* 289: 18189–18201
- Jha P, Claudel T, Baghdasaryan A, Mueller M, Halilbasic E, Das SK, Lass A, Zimmermann R, Zechner R, Hoefler G et al (2014) Role of adipose triglyceride lipase (PNPLA2) in protection from hepatic inflammation in mouse models of steatohepatitis and endotoxemia. *Hepatology* 59: 858–869
- Kandyba E, Leung Y, Chen YB, Widelitz R, Chuong CM, Kobiela K (2013) Competitive balance of intrabulge BMP/Wnt signaling reveals a robust gene network ruling stem cell homeostasis and cyclic activation. *Proc Natl Acad Sci USA* 110: 1351–1356
- Kashgari G, Meinecke L, Gordon W, Ruiz B, Yang J, Ma AL, Xie Y, Ho H, Plikus MV, Nie Q et al (2020) Epithelial migration and non-adhesive periderm are required for digit separation during mammalian development. *Dev Cell* 52: 764–778.e4
- Keyes BE, Liu S, Asare A, Naik S, Levorse J, Polak L, Lu CP, Nikolova M, Pasolli HA, Fuchs E (2016) Impaired epidermal to dendritic T cell signaling slows wound repair in aged skin. *Cell* 167: 1323–1338.e14
- Kim YJ, Ryu HM, Choi JY, Cho JH, Kim CD, Park SH, Kim YL (2017) Hypoxanthine causes endothelial dysfunction through oxidative stress-induced apoptosis. *Biochem Biophys Res Commun* 482: 821–827
- Kishibe M (2014) Kallikrein-related peptidase 8 (KLK8): the structure and function in the epidermis. *J Dermatolog Clin Res* 2: 1030
- Klicznik MM, Szenes-Nagy AB, Campbell DJ, Gratz IK (2018) Taking the lead – how keratinocytes orchestrate skin T cell immunity. *Immunol Lett* 200: 43–51
- Koenecke C, Chennupati V, Schmitz S, Malissen B, Förster R, Prins I (2009) In vivo application of mAb directed against the  $\gamma\delta$  TCR does not deplete but generates “invisible”  $\gamma\delta$  T cells. *Eur J Immunol* 39: 372–379
- Koster MI (2009) Making an epidermis. *Ann N Y Acad Sci* 1170: 7–10
- Kubo A, Nagao K, Yokouchi M, Sasaki H, Amagai M (2009) External antigen uptake by Langerhans cells with reorganization of epidermal tight junction barriers. *J Exp Med* 206: 2937–2946
- Kuleshov MV, Jones MR, Rouillard AD, Fernandez NF, Duan Q, Wang Z, Koplev S, Jenkins SL, Jagodnik KM, Lachmann A et al (2016) Enrichr: a comprehensive gene set enrichment analysis web server 2016 update. *Nucleic Acids Res* 44: W90–W97
- Langmead B, Salzberg SL (2012) Fast gapped-read alignment with bowtie 2. *Nat. Methods* 9: 357–359
- Lay K, Yuan S, Gur-Cohen S, Miao Y, Han T, Naik S, Pasolli HA, Larsen SB, Fuchs E (2018) Stem cells repurpose proliferation to contain a breach in their niche barrier. *Elife* 7: e41661
- Lee B, Villarreal-Ponce A, Fallahi M, Ovadia J, Sun P, Yu QC, Ito S, Sinha S, Nie Q, Dai X (2014a) Transcriptional mechanisms link epithelial plasticity to adhesion and differentiation of epidermal progenitor cells. *Dev Cell* 29: 47–58
- Lee MJ, Pramyothin P, Karastergiou K, Fried SK (2014b) Deconstructing the roles of glucocorticoids in adipose tissue biology and the development of central obesity. *Biochim Biophys Acta* 1842: 473–481
- Lee Y, Song YS, Fang CH, So BI, Park JY, Joo HW, Park IH, Shen GY, Shin JH, Kim H et al (2014c) Anti-obesity effects of granulocyte-Colony stimulating factor in Otsuka-long-Evans-Tokushima fatty rats. *PLoS One* 9: 105603
- Lin Z, Jin S, Chen J, Li Z, Lin Z, Tang L, Nie Q, Andersen B (2020) Murine interfollicular epidermal differentiation is gradualistic with GRHL3 controlling progression from stem to transition cell states. *Nat Commun* 11: 1–15
- Lind EF, Ahonen CL, Wasiuk A, Kosaka Y, Becher B, Bennett KA, Noelle RJ (2008) Dendritic cells require the NF- $\kappa$ B2 pathway for cross-presentation of soluble antigens. *J Immunol* 181: 354–363
- Liu J, Cao S, Kim S, Chung EY, Homma Y, Guan X, Jimenez V, Ma X (2005) Interleukin-12: an update on its immunological activities, signaling and regulation of gene expression. *Curr Immunol Rev* 1: 119–137
- Love MI, Huber W, Anders S (2014) Moderated estimation of fold change and dispersion for RNA-seq data with DESeq2. *Genome Biol* 15: 550
- MacKay DR, Hu M, Li B, Rhéaume C, Dai X (2006) The mouse *Ovol2* gene is required for cranial neural tube development. *Dev Biol* 291: 38–52
- Mair F, Joller S, Hoeppli R, Onder L, Hahn M, Ludewig B, Waisman A, Becher B (2015) The NF $\kappa$ B-inducing kinase is essential for the developmental programming of skin- resident and IL-17-producing  $\Gamma\delta$  T $\delta$  cells. *Elife* 4: e10087
- Manuel Sánchez-Maldonado J, Martínez-Bueno M, Canhão H, ter Horst R, Muñoz-Peña S, Moñiz-Díez A, Rodríguez-Ramos A, Escudero A, Sorensen SB, Hetland ML et al (2020) NFKB2 polymorphisms associate with the risk of developing rheumatoid arthritis and response to TNF inhibitors: results from the REPAIR consortium. *Sci Rep* 10: 4316
- Marenholz I, Esparza-Gordillo J, Rüschemdorf F, Bauerfeind A, Strachan DP, Spycher BD, Baurecht H, Margaritte-Jeannin P, Sääf A, Kerkhof M et al (2015) Meta-analysis identifies seven susceptibility loci involved in the atopic march. *Nat Commun* 6: 8804
- Matsushita M, Nirengi S, Hibi M, Wakabayashi H, Lee SI, Domichi M, Sakane N, Saito M (2021) Diurnal variations of brown fat thermogenesis and fat oxidation in humans. *Int J Obes* 45: 2499–2505
- Mendoza-Reinoso V, Beverdam A (2018) Epidermal YAP activity drives canonical WNT16/ $\beta$ -catenin signaling to promote keratinocyte proliferation in vitro and in the murine skin. *Stem Cell Res* 29: 15–23
- Merad M, Ginhoux F, Collin M (2008) Origin, homeostasis and function of Langerhans cells and other langerin-expressing dendritic cells. *Nat Rev Immunol* 8: 935–947
- Moore KS, Moore R, Fulmer DB, Guo L, Gensemer C, Stairley R, Glover J, Beck TC, Morningstar JE, Biggs R et al (2022) DCHS1, Lix1L, and the septin cytoskeleton: molecular and developmental etiology of mitral valve prolapse. *J Cardiovasc Dev Dis* 9: 62
- Moretti L, Stalfort J, Barker TH, Abeyayehu D (2022) The interplay of fibroblasts, the extracellular matrix, and inflammation in scar formation. *J Biol Chem* 298: 101530

- Moulin V, Tam BYY, Castilloux G, Auger FA, O'Connor-McCourt MD, Philip A, Germain L (2001) Fetal and adult human skin fibroblasts display intrinsic differences in contractile capacity. *J Cell Physiol* 188: 211–222
- Mowers J, Uhm M, Reilly SM, Simon J, Leto D, Chiang SH, Chang L, Saltiel AR (2013) Inflammation produces catecholamine resistance in obesity via activation of PDE3B by the protein kinases IKK $\epsilon$  and TBK1. *Elife* 2: e01119
- Naik S, Fuchs E (2022) Inflammatory memory and tissue adaptation in sickness and in health. *Nature* 607: 249–255
- Nair M, Teng A, Bilanchone V, Agrawal A, Li B, Dai X (2006) *Ovol1* regulates the growth arrest of embryonic epidermal progenitor cells and represses c-myc transcription. *J Cell Biol* 173: 253–264
- Natsuga K (2014) Epidermal barriers. *Cold Spring Harb Perspect Med* 4: a018218
- Nauroy P, Nyström A (2020) Kallikreins: essential epidermal messengers for regulation of the skin microenvironment during homeostasis, repair and disease. *Matrix Biol Plus* 6–7: 100019
- Niec RE, Rudensky AY, Fuchs E (2021) Inflammatory adaptation in barrier tissues. *Cell* 184: 3361–3375
- Nishibu A, Ward BR, Jester JV, Ploegh HL, Boes M, Takashima A (2006) Behavioral responses of epidermal Langerhans cells *In situ* to local pathological stimuli. *J Invest Dermatol* 126: 787–796
- O'Brien RL, Born WK (2015) Dermal  $\gamma\delta$  T cells – what have we learned? *Cell Immunol* 296: 62–69
- Oh H, Ghosh S (2013) NF- $\kappa$ B: roles and regulation in different CD4+ T cell subsets. *Immunol Rev* 252: 41–51
- Oji V, Eckl KM, Aufenvenne K, Nätebus M, Tarinski T, Ackermann K, Seller N, Metzke D, Nürnberg G, Fölster-Holst R et al (2010) Loss of corneodesmosin leads to severe skin barrier defect, pruritus, and atopy: unraveling the peeling skin disease. *Am J Hum Genet* 87: 274–281
- de Oliveira EM, Silva JC, Ascar TP, Sandri S, Marchi AF, Migliorini S, Nakaya HTI, Fock RA, Campa A (2022) Acute inflammation is a predisposing factor for weight gain and insulin resistance. *Pharmaceutics* 14: 623
- Oppmann B, Lesley R, Blom B, Timans JC, Xu Y, Hunte B, Vega F, Yu N, Wang J, Singh K et al (2000) Novel p19 protein engages IL-12p40 to form a cytokine, IL-23, with biological activities similar as well as distinct from IL-12. *Immunity* 13: 715–725
- Oranges T, Dini V, Romanelli M (2015) Skin physiology of the neonate and infant: clinical implications. *Adv Wound Care* 4: 587–595
- Park S, Matte-Martone C, Gonzalez DG, Lathrop EA, May DP, Pineda CM, Moore JL, Boucher JD, Marsh E, Schmitter-Sánchez A et al (2021) Skin-resident immune cells actively coordinate their distribution with epidermal cells during homeostasis. *Nat. Cell Biol* 235: 476–484
- Patel S, Xi ZF, Seo EY, McGaughey D, Segre JA (2006) Klf4 and corticosteroids activate an overlapping set of transcriptional targets to accelerate *in utero* epidermal barrier acquisition. *Proc Natl Acad Sci USA* 103: 18668–18673
- Paternoster L, Standl M, Chen CM, Ramasamy A, Bønnelykke K, Duijts L, Ferreira MA, Alves AC, Thyssen JP, Albrecht E et al (2011) Meta-analysis of genome-wide association studies identifies three new risk loci for atopic dermatitis. *Nat Genet* 44: 187–192
- Peckett AJ, Wright DC, Riddell MC (2011) The effects of glucocorticoids on adipose tissue lipid metabolism. *Metabolism* 60: 1500–1510
- Pfitzenmaier J, Vessella R, Higano CS, Noteboom JL, Wallace D, Corey E (2003) Elevation of cytokine levels in cachectic patients with prostate carcinoma. *Cancer* 97: 1211–1216
- Proksch E, Fölster-Holst R, Jensen JM (2006) Skin barrier function, epidermal proliferation and differentiation in eczema. *J Dermatol Sci* 43: 159–169
- Qi F, Isaji T, Duan C, Yang J, Wang Y, Fukuda T, Gu J (2020) ST3GAL3, ST3GAL4, and ST3GAL6 differ in their regulation of biological functions via the specificities for the  $\alpha$ 2,3-sialylation of target proteins. *FASEB J* 34: 881–897
- Rada-Iglesias A, Bajpai R, Swigut T, Brugmann SA, Flynn RA, Wysocka J (2011) A unique chromatin signature uncovers early developmental enhancers in humans. *Nature* 470: 279–283
- Ramos-Jiménez A, Hernández-Torres RP, Torres-Durán PV, Romero-Gonzalez J, Mascher D, Posadas-Romero C, Juárez-Oropeza MA (2008) The respiratory exchange ratio is associated with fitness indicators both in trained and untrained men: a possible application for people with reduced exercise tolerance. *Clin Med Circ Respirat Pulm Med* 2: 1–9
- Redd L, Schmelz M, Burack WR, Cook JR, Day AW, Rimsza L (2016) Langerhans cell histiocytosis shows distinct cytoplasmic expression of major histocompatibility class II antigens. *J Hematop* 9: 107–112
- Richardson GD, Bazzi H, Fantauzzo KA, Waters JM, Crawford H, Hynd P, Christiano AM, Jahoda CAB (2009) KGF and EGF signalling block hair follicle induction and promote interfollicular epidermal fate in developing mouse skin. *Development* 136: 2153–2164
- Rognoni E, Pisco AO, Hiratsuka T, Sipilä KH, Belmonte JM, Mobasser SA, Philippeos C, Dilão R, Watt FM (2018) Fibroblast state switching orchestrates dermal maturation and wound healing. *Mol Syst Biol* 14: e8174
- Sakabe JI, Yamamoto M, Hirakawa S, Motoyama A, Ohta I, Tatsuno K, Ito T, Kabashima K, Hibino T, Tokura Y (2013) Kallikrein-related peptidase 5 functions in proteolytic processing of Proflaggrin in cultured human keratinocytes. *J Biol Chem* 288: 17179–17189
- Sampath H, Flowers MT, Liu X, Paton CM, Sullivan R, Chu K, Zhao M, Ntambi JM (2009) Skin-specific deletion of stearoyl-CoA desaturase-1 alters skin lipid composition and protects mice from high fat diet-induced obesity. *J Biol Chem* 284: 19961–19973
- Sandilands A, Sutherland C, Irvine AD, McLean WHI (2009) Filaggrin in the frontline: role in skin barrier function and disease. *J Cell Sci* 122: 1285–1294
- Sandrock I, Reinhardt A, Ravens S, Binz C, Wilharm A, Martins J, Oberdörfer L, Tan L, Lienenklaus S, Zhang B et al (2018) Genetic models reveal origin, persistence and non-redundant functions of IL-17–producing  $\gamma\delta$  T cells. *J Exp Med* 215: 3006–3018
- Sano S (2015) Psoriasis as a barrier disease. *Dermatol Sin* 33: 64–69
- Schindelin J, Arganda-Carreras I, Frise E, Kaynig V, Longair M, Pietzsch T, Preibisch S, Rueden C, Saalfeld S, Schmid B et al (2012) Fiji: an open-source platform for biological-image analysis. *Nat Methods* 9: 676–682
- Schmuth M, Blunder S, Dubrac S, Gruber R, Moosbrugger-Martinez V (2015) Epidermal barrier in hereditary ichthyoses, atopic dermatitis, and psoriasis. *J Dtsch Dermatol Ges* 13: 1119–1123
- Segre JA (2006) Epidermal barrier formation and recovery in skin disorders. *J Clin Invest* 116: 1150–1158
- Sethi I, Gluck C, Zhou H, Buck MJ, Sinha S (2017) Evolutionary re-wiring of p63 and the epigenomic regulatory landscape in keratinocytes and its potential implications on species-specific gene expression and phenotypes. *Nucleic Acids Res* 45: 8208–8224
- Sha Y, Haensel D, Gutierrez G, Du H, Dai X, Nie Q (2019) Intermediate cell states in epithelial-to-mesenchymal transition. *Phys Biol* 16: 021001
- Sherwood LM, Parris EE, Cahill GF (1970) Starvation in man. *N Engl J Med* 282: 668–675
- Škop V, Guo J, Liu N, Xiao C, Hall KD, Gavrilo O, Reitman ML (2020) Mouse thermoregulation: introducing the concept of the thermoneutral point. *Cell Rep* 31: 107501
- Speakman JR (2013) Measuring energy metabolism in the mouse – theoretical, practical, and analytical considerations. *Front Physiol* 4: 34
- Spicuglia S, Vanhille L (2012) Chromatin signatures of active enhancers. *Nucleus* 3: 126–131

- Sulcova J, Maddaluno L, Meyer M, Werner S (2015) Accumulation and activation of epidermal  $\gamma\delta$  T cells in a mouse model of chronic dermatitis is not required for the inflammatory phenotype. *Eur J Immunol* 45: 2517–2528
- Sumaria N, Roediger B, Ng LG, Qin J, Pinto R, Cavanagh LL, Shklovskaya E, Barbara BF, Triccas JA, Weninger W (2011) Cutaneous immunosurveillance by self-renewing dermal  $\gamma\delta$  T cells. *J Exp Med* 208: 505–518
- Sun P, Vu R, Dragan M, Haensel D, Gutierrez G, Nguyen Q, Greenberg E, Chen Z, Wu J, Atwood S et al (2021) OVOL1 regulates psoriasis-like skin inflammation and epidermal hyperplasia. *J Invest Dermatol* 141: 1542–1552
- Suzuki T, Okada Y, Sembat S, Orba Y, Yamanouchi S, Endo S, Tanaka S, Fujita T, Kuroda S, Nagashima K et al (2005) Identification of FEZ1 as a protein that interacts with JC virus agnoprotein and microtubules: role of agnoprotein-induced dissociation of FEZ1 from microtubules in viral propagation. *J Biol Chem* 280: 24948–24956
- Tanaka T, Narazaki M, Kishimoto T (2014) IL-6 in inflammation, immunity, and disease. *Cold Spring Harb Perspect Biol* 6: 16295–16296
- Tang A, Amagai M, Granger LG, Stanley JR, Uddy MC (1993) Adhesion of epidermal Langerhans cells to keratinocytes mediated by E-cadherin. *Nature* 361: 82–85
- Teng A, Nair M, Wells J, Segre JA, Dai X (2007) Strain-dependent perinatal lethality of *Ovol1*-deficient mice and identification of *Ovol2* as a downstream target of *Ovol1* in skin epidermis. *Biochim Biophys Acta* 1772: 89–95
- Tsuji G, Hashimoto-Hachiya A, Kiyomatsu-Oda M, Takemura M, Ohno F, Ito T, Morino-Koga S, Mitoma C, Nakahara T, Uchi H et al (2017) Aryl hydrocarbon receptor activation restores filaggrin expression via *OVOL1* in atopic dermatitis. *Cell Death Dis* 8: e2931
- Ueta C, Kawasumi H, Fujiwara H, Miyagawa T, Kida H, Ohmoto Y, Kishimoto S, Tsuyuguchi I (1996) Interleukin-12 activates human gamma delta T cells: synergistic effect of tumor necrosis factor- $\alpha$ . *Eur J Immunol* 26: 3066–3073
- Unzaki S, Horai R, Sudo K, Iwakura Y, Ito S (2007) *Ovol2/Movo*, a homologue of *Drosophila ovo*, is required for angiogenesis, heart formation and placental development in mice. *Genes Cells* 12: 773–785
- Van den Bossche J, Van Ginderachter JA (2013) E-cadherin: from epithelial glue to immunological regulator. *Eur J Immunol* 43: 34–37
- Vasioukhin V, Degenstein L, Wise B, Fuchs E (1999) The magical touch: genome targeting in epidermal stem cells induced by tamoxifen application to mouse skin. *Proc Natl Acad Sci USA* 96: 8551–8556
- Völlner F, Ali J, Kurrle N, Exner Y, Eming R, Hertl M, Banning A, Tikkanen R (2016) Loss of flotillin expression results in weakened desmosomal adhesion and pemphigus vulgaris-like localisation of desmoglein-3 in human keratinocytes. *Sci Rep* 6: 28820
- Vu R, Dragan M, Sun P, Werner S, Dai X (2022a) Epithelial-mesenchymal plasticity and endothelial-mesenchymal transition in cutaneous wound healing. *Cold Spring Harb Perspect Biol* <https://doi.org/10.1101/cshperspect.a041237>
- Vu R, Jin S, Sun P, Haensel D, Nguyen QH, Dragan M, Kessenbrock K, Nie Q, Dai X (2022b) Wound healing in aged skin exhibits systems-level alterations in cellular composition and cell-cell communication. *Cell Rep* 40: 111155
- Vulcano M, Albanesi C, Stoppacciaro A, Bagnati R, D'Amico G, Struyf S, Transidico P, Bonocchi R, Del Prete A, Allavena P et al (2001) Dendritic cells as a major source of macrophage-derived chemokine/CCL22 in vitro and in vivo. *Eur J Immunol* 31: 812–822
- Wang XP, Schunck M, Kallen KJ, Neumann C, Trautwein C, Rose-John S, Proksch E (2004) The Interleukin-6 cytokine system regulates epidermal permeability barrier homeostasis. *J Invest Dermatol* 123: 124–131
- Wang X, Enomoto A, Weng L, Mizutani Y, Abudureyimu S, Esaki N, Tsuyuki Y, Chen C, Mii S, Asai N et al (2018) Girdin/GIV regulates collective cancer cell migration by controlling cell adhesion and cytoskeletal organization. *Cancer Sci* 109: 3643–3656
- Watanabe K, Villarreal-Ponce A, Sun P, Salmans ML, Fallahi M, Andersen B, Dai X (2014) Mammary morphogenesis and regeneration require the inhibition of EMT at terminal end buds by *ovol2* transcriptional repressor. *Dev Cell* 29: 59–74
- Wells J, Lee B, Cai AQ, Karapetyan A, Lee WJ, Rugg E, Sinha S, Nie Q, Dai X (2009) *Ovol2* suppresses cell cycling and terminal differentiation of keratinocytes by directly repressing *c-Myc* and *Notch1*. *J Biol Chem* 284: 29125–29135
- Wu X, Zhao J, Ruan Y, Sun L, Xu C, Jiang H (2018) Sialyltransferase ST3GAL1 promotes cell migration, invasion, and TGF- $\beta$ 1-induced EMT and confers paclitaxel resistance in ovarian cancer. *Cell Death Dis* 9: 1102
- Xie Z, Bailey A, Kuleshov MV, Clarke DJB, Evangelista JE, Jenkins SL, Lachmann A, Wojciechowicz ML, Kropiwnicki E, Jagodnik KM et al (2021) Gene set knowledge discovery with Enrichr. *Curr Protoc* 1: e90
- Xiong Y, Bosselut R (2012) CD4-CD8 differentiation in the thymus: connecting circuits and building memories. *Curr Opin Immunol* 24: 139–145
- Yamamoto H, Hattori M, Chamulitrat W, Ohno Y, Kihara A (2020) Skin permeability barrier formation by the ichthyosis-causative gene *FATP4* through formation of the barrier lipid  $\omega$ -O-acylceramide. *Proc Natl Acad Sci USA* 117: 2914–2922
- Yan B, Liu N, Li J, Li J, Zhu W, Kuang Y, Chen X, Peng C (2020) The role of Langerhans cells in epidermal homeostasis and pathogenesis of psoriasis. *J Cell Mol Med* 24: 11646–11655
- Yang R, Yao L, Shen L, Sha W, Modlin RL, Shen H, Chen ZW (2019) IL-12 expands and differentiates human  $V\gamma 2V\delta 2$  T effector cells producing antimicrobial cytokines and inhibiting intracellular mycobacterial growth. *Front Immunol* 10: 913
- Yang J, Antin P, Bex G, Blanpain C, Brabletz T, Bronner M, Campbell K, Cano A, Casanova J, Christofori G et al (2020) Guidelines and definitions for research on epithelial-mesenchymal transition. *Nat Rev Mol Cell Biol* 21: 341–352
- Yang F, Yang L, Teng L, Zhang H, Katayama I (2021) Morphological alterations and increased S100B expression in epidermal Langerhans cells detected in skin from patients with progressive vitiligo. *Life* 11: 579
- Yoo JK, Cho JH, Lee SW, Sung YC (2002) IL-12 provides proliferation and survival signals to murine CD4+ T cells through phosphatidylinositol 3-kinase/Akt signaling pathway. *J Immunol* 169: 3637–3643
- Yoshimura SI, Gerondopoulos A, Linford A, Rigden DJ, Barr FA (2010) Family-wide characterization of the DENN domain Rab GDP-GTP exchange factors. *J Cell Biol* 191: 367–381
- Zhang Y, Liu T, Meyer CA, Eeckhoutte J, Johnson DS, Bernstein BE, Nussbaum C, Myers RM, Brown M, Li W et al (2008) Model-based analysis of ChIP-Seq (MACS). *Genome Biol* 9: R137
- Zhang Z, Jiang Y, Su L, Ludwig S, Zhang X, Tang M, Li X, Anderton P, Zhan X, Choi M et al (2022) Obesity caused by an *OVOL2* mutation reveals dual roles of *OVOL2* in promoting thermogenesis and limiting white adipogenesis. *Cell Metab* 34: 1860–1874.e4
- Zheng T (2014) The atopic march: progression from atopic dermatitis to allergic rhinitis and asthma. *J Clin Cell Immunol* 3: 67–73



**License:** This is an open access article under the terms of the [Creative Commons Attribution-NonCommercial-NoDerivs](https://creativecommons.org/licenses/by-nc-nd/4.0/) License, which permits use and distribution in any medium, provided the original work is properly cited, the use is non-commercial and no modifications or adaptations are made.